Gradients in cellular metabolism regulate development of tonotopy along the cochlea

Thomas S Blacker [2#], James DB O'Sullivan [1#], Val Yianni [1], Mohi Ahmed [1], Zoe F Mann [1*].

[1] Centre for Craniofacial and Regenerative Biology, King's College London, SE1 9RT, United Kingdom.

[2]Department of Physics and Astronomy, University College London, WC1E 6BT United Kingdom.

[#] Equal primary author contribution

* Corresponding author: zoe.mann@kcl.ac.uk

Zoë F Mann, Ph.D
Centre for Craniofacial and Regenerative Biology
Faculty of Dentistry, Oral & Craniofacial Sciences
Guy's Hospital
Great Maze Road
London SE1 1UK, U.K.

Gradients in cellular metabolism regulate development of tonotopy along the cochlea

Thomas S Blacker [2#], James DB O'Sullivan [1#], Val Yianni [1], Mohi Ahmed [1], Zoe F Mann [1*].

[1] Centre for Craniofacial and Regenerative Biology, King's College London

[2] Department of Physics and Astronomy, University College London

[#] Equal primary author contribution

Corresponding author: zoe.mann@kcl.ac.uk

Abstract

In vertebrates with elongated auditory organs, mechanosensory hair cells (HCs) are organised such that complex sounds are broken down into their component frequencies along the basal-to-apical long (tonotopic) axis. To generate the frequency-specific characteristics required at the appropriate positions, nascent HCs must determine their tonotopic properties during development. This relies on complex signalling between the developing HC and its local niche along the axis within the auditory organ. Here we apply NAD(P)H fluorescence lifetime imaging (FLIM) and live imaging of mitochondria to reveal metabolic gradients along the tonotopic axis of the developing cochlea. We further show that re-shaping these gradients during development, by inhibiting cytosolic glucose metabolism, alters normal Bmp7 and Chordin like-1 signalling leading to flattening of tonotopic patterning along the axis. Our work supports a causal link between morphogen signalling and metabolic reprogramming in specifying tonotopic morphologies in auditory HCs.

Introduction

Hearing relies on the life-long function of mechanosensory hair cells (HCs) and their associated glial-like supporting cells (SCs). In both mammals and birds, complex sounds are separated into component frequencies by the anatomy of the cochlea, so that different frequencies stimulate HCs located at different positions along the basal-to-apical long axis of the epithelium (tonotopy). This phenomenon underlies our ability to differentiate between the high pitch of a mosquito and the low rumbling of thunder. The specific factors regulating tonotopy remain, largely, unclear. A better understanding of how specific factors regulate tonotopy and, therefore, the formation of frequency-specific HC phenotypes will provide insights regarding both congenital auditory defects and HC regeneration. In particular, high frequency HCs show increased vulnerability to insults, including aging [1], noise damage [2,3] and ototoxicity [4]. Therefore, information regarding the pathways that specify this HC phenotype could identify potential methods to preserve these cells and/or recover high frequency hearing loss.

Metabolism, encompassing the complex network of chemical reactions that sustain life, has emerged as a key regulator of cell fate and differentiation [5]. Instructive roles for glucose metabolism and reprogramming between glycolytic and oxidative pathways has been reported in various systems during development including, for example, delamination and migration in embryonic neural crest [6], hair cells in the zebrafish inner ear [7], specification of trophectoderm fate in the mouse embryo [8] and cell fate decisions along the developing body axis [9-11]. As a complex tissue containing multiple cell types, investigating how metabolism regulates HC formation within the cochlear niche requires experimental approaches capable of interrogating metabolic pathways in live preparations, with single cell resolution. The classic biochemical approaches from which our knowledge of metabolism has formed involve the destructive extraction of metabolites from a sample for subsequent analysis. Probing metabolism in this way, although valuable, means that the spatial organisation of complex tissues is lost. We have previously exploited the intrinsic fluorescence of reduced nicotinamide

adenine dinucleotide (NADH) and its phosphorylated analog NADPH to investigate the metabolic state in HCs and SCs cells of mature cochlear preparations during aging and ototoxicity [12,13]. Both NADH and NADPH serve as reporters of metabolism because they function as redox regulators, transporting reducing equivalents between the enzyme-catalysed reactions of cellular metabolism. Reprogramming of metabolic pathways in tissues causes changes in the time-resolved properties of the NAD(P)H fluorescence signal [14]. Fluorescence lifetime imaging (FLIM) of cellular NAD(P)H therefore provides a non-invasive and label-free method with which to probe metabolism at the single cell level throughout cochlear development [15], an area which is largely unexplored.

Using previously defined morphological markers of tonotopy as read-outs for HC phenotype [16,17] we here investigate a role for metabolism in specifying proximal (high frequency) verses distal (low frequency) HCs. We first identify a gradient in NADPH-linked metabolism along the tonotopic axis of the developing chick cochlea. This gradient is then further confirmed through analysis of metabolic mRNAs and the expression patterns of metabolic effector proteins along the tonotopic axis. We functionally test the role of these gradients by modulating metabolic flux through different branches of glucose metabolism at key stages in HC formation. We find that glucose flux specifically through the pentose phosphate pathway (PPP) instructs tonotopic HC morphologies, by regulating the graded expression of Bmp7 and its antagonist Chordin-like-1, known determinants of tonotopic identity [18]. We also characterise metabolic differences and the timing of this divergence in nascent HCs and SCs. Our findings highlight a novel role for cytosolic glucose metabolism in specifying HC positional identity and provide the first characterisation of unique metabolic states associated with the emergence of HC and SC lineages.

Results

NAD(P)H FLIM reveals differences in the cellular balance of NADPH to NADH along the tonotopic axis of the developing BP.

NAD(P)H FLIM studies in live cells and tissues resolve two fluorescence lifetimes (Figure 1A-D); one with a duration of around 0.4 ns from freely diffusing NAD(P)H (labelled τ_{free}) and the other of 2 ns or more from the pool of NAD(P)H that is bound to enzymes (τ_{bound}) [19,20] (Figure 1C). We have previously shown that the lifetime of enzyme bound (phosphorylated) NADPH is significantly longer than that of bound (unphosphorylated) NADH [14,21]. Changes in τ_{bound} therefore report changes in the cellular NADPH/NADH ratio [12], providing a direct readout of metabolic alterations in living cells. We used this to monitor metabolism along the proximal-to-distal (tonotopic) axis of the BP, both during development and between cell types (Figure 1E-H). At E6 and we observed a significant ($p < 0.05$, Student's *t*-test) difference in τ_{bound} along the tonotopic axis (Figure 1D-I). The proximal-to-distal gradient in τ_{bound} (Figure 1D) was still present at E14, at which time HCs are considered fully differentiated (Figure 1G-J) ($p < 0.05$, Student's *t*-test). In contrast, the gradient was absent at E16. The increased τ_{bound} in the proximal compared to distal BP corresponds to a gradient in metabolic activity along the tonotopic axis between E6 and E14. This suggests that NADPH-producing pathways may regulate developmental refinement of HCs along the tonotopic axis rather than playing a role in their physiological frequency responses, which are apparent from E16 onwards.

FLIM also yields the relative abundance of the bound and free NAD(P)H populations, labelled α_{bound}. Changes in this parameter in response to a range of metabolic perturbations have also been observed[19,22], raising hope of its use as a complementary readout of metabolic state. At present, however, the biochemical relationships linking α_{bound} to metabolic phenotype are less established than for τ_{bound}. Nevertheless, it is thought that α_{bound} reports shifts in the balance between glycolytic and oxidative ATP production, where a lower α_{bound} reflects a more glycolytic phenotype [19]. Based on this

hypothesis, the changes in α_{bound} observed here would indicate dynamic shifts between glycolytic and oxidative pathways throughout BP development (Figure 1J).

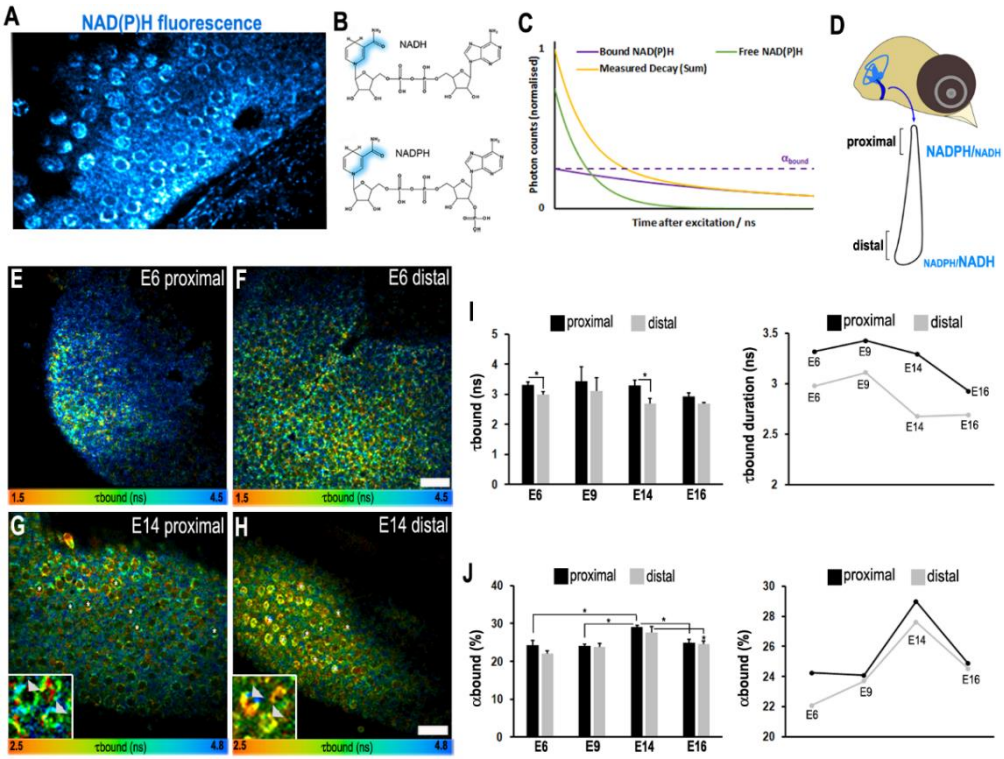

Figure 1. A proximal-to-distal metabolic gradient in the developing chick cochlea.
(A) Two-photon fluorescence image showing NAD(P)H in a live BP explant at E14.
(B) Inherent fluorescence from NADH and NADPH results from redistribution of electronic charge across the amide group of the reduced nicotinamide ring.
(C) NAD(P)H FLIM resolves two components corresponding to freely diffusing (shorter lifetime, τ_{free}) and enzyme bound (longer lifetime, τ_{bound}). The relative proportion of these components is labelled α_{bound}. Changes in τ_{bound} and α_{bound} imply changes in metabolic state.
(D) Schematic of the chick BP, showing the progressive change in the NADPH/NADH ratio along the tonotopic axis of the BP.
(E-H) FLIM images of the NAD(P)H fluorescence lifetime signal extracted for τ_{bound} in the proximal and distal BP regions at E6 and E14. The mean lifetime signal is ($\tau_m = (1 - \alpha_{bound})\tau_{free} + \alpha_{bound}\tau_{free}$). A proximal-to-distal gradient is evident in τ_{bound} but not α_{bound} throughout BP development. White asterisks indicate the HCs. Higher magnification images highlight the differences in mean lifetime between proximal and distal HCs at E14.
(I) Quantification of τ_{bound} during development shows a shift from NADPH to NADH producing pathways. Line graphs highlight differences in τ_{bound} between proximal (black) and distal (grey) BP regions throughout development.
(J) α_{bound}, reflecting the cellular balance between free and enzyme-bound NAD(P)H, increases significantly in both proximal (black) and distal (grey) BP regions between E6 and E14 and decreases significantly between E14 and E16. Line graphs show differences in α_{bound} in the proximal (black) and distal (grey) regions.
The difference in mean NAD(P)H lifetime result from a shift in the cellular balance of NADPH/NADH, and thus in utilisation of the metabolic pathways that produce these cofactors, from high to low frequency regions. Scale bars = 50µm. Data are mean ± SEM; E6: n = 6, E9: n= 4, E14: n = 7 and E16: n = 6 biological replicates. ***** $p < 0.05$ Student's *t*-test.

As HCs and SCs are not easily identified at stages before E9 (Figure 1 E, F), the NAD(P)H FLIM data were initially analysed from the whole epithelium along the proximal to distal axis. However, at E14 and E16 we were able to specifically examine τ_{bound} and α_{bound} in HCs and SCs (Figure 2A, B). We found

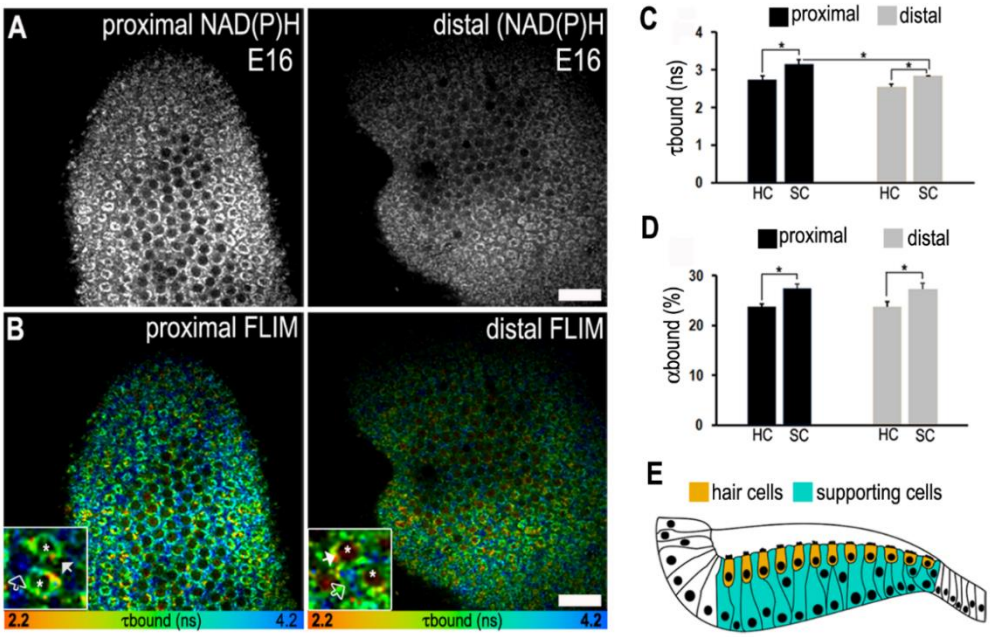

Figure 2. Metabolic differences between hair cells and supporting cells along the tonotopic axis of the developing chick cochlea.
(A) Total NAD(P)H fluorescence in the proximal and distal regions of the BP at E16.
(B) Mean fluorescence lifetime signal for NAD(P)H in the proximal and distal BP. Images show the lifetime signal for bound NAD(P)H and are mapped using a pseudo colour time scale representing a duration of 2.2 and 4.2 ns. White boxes show the differences in mean lifetime between hair cells (white asterisk, block arrows) and supporting cells (empty arrows).
(C) At E16, τbound is significantly higher in supporting cells compared to hair cells, indicating distinct metabolic profiles between cell types. The hair-cell-to-supporting cell difference in τbound is higher in the proximal (black bars) compared to distal (grey bars) BP region.
(D) The cellular proportion of bound NAD(P)H (αbound) is significantly higher in supporting compared to hair cells again reflecting the cell-specific differences in metabolic pathway utilisation.
(E) Schematic showing a cross-sectional view of the BP at E16. The hair cells (orange) and supporting cells (blue) are indicated. Colours reflect the bound lifetime duration in ns shown in (B). Warm colours indicate short lifetimes and cool colours longer lifetimes.
Data are mean ± SEM. * $p < 0.05$, Student's paired *t*-test, n = 10 biological replicates. Scale bars are 50μm.

that both parameters differed significantly between cell types at all positions along the proximal-to-distal axis (Figure 2C, D, E). Additionally, the axial gradient in τ_{bound} (NADPH/NADH ratio) (Figure 2C) in SCs but not HCs is consistent with our results from whole epithelial measurements at E6 and E14 (Figure 1E-J), showing the same metabolic differences as a function of tonotopic position along the cochlea.

Differential expression of mRNAs regulating NADPH production along the tonotopic axis.
Having identified a gradient in the cellular balance of NADPH/NADH along the BP at E6, we sought to determine the metabolic pathways underlying the differences in τ_{bound} and α_{bound}. By exploiting our previously generated bulk RNA-seq and Affymetrix microarray data sets [18] we measured differential expression of metabolic mRNAs along the BP at E6.5 and E14 (Figure 3). In these experiments, BPs had been separated, for bulk RNA-seq and Affymetrix microarray analysis, into proximal, middle, and distal thirds prior to isolation of mRNA [18]. Microarray data were analysed to identify transcripts with expression levels at least two-fold higher in the proximal compared to distal half of the BP. We identified multiple genes with differential expression between proximal and distal regions that

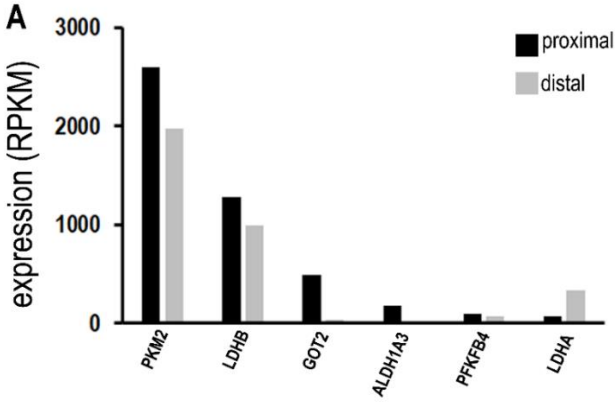

B

E6.5			
Gene	Proximal	Distal	Log_2
ALDH1A3	177.65	9.26	-4.6
GOT2	481.83	29.36	-0.7
LDHB	1277.25	993.42	-0.3
PFKFB4	93.61	70.87	-0.4
PKM2	2591.581	1979.26	-0.3
LDHA	70.16	333.28	2.24

C

E14	
Gene	Fold change
ALDH1A3	19
GOT2	1.6
NNT	1.5
IDH3B	1.4
IDH3A	-1.6

Figure 3. Differential expression of mRNAs encoding NADPH and NADH regulatory enzymes in the chick basilar papilla.
(A-B) Bulk RNA-seq data showing differential expression of genes that regulate the cellular NADPH/NADH ratio. Data show the normalised RPKM values in the proximal and distal BP regions at E6.5 (normalised reads per kilobase of transcript per million mapped reads). All genes with a Log_2 >1 are significantly expressed in the distal BP region and all genes with a Log_2 <1 are expressed significantly in the proximal BP region. Statistical significance levels were calculated by one-way ANOVA. For a gene to be considered 'differential', at least one region of the BP (proximal, middle or distal) was required to be ≥ 0.5 RPKM. A fold change of ≥ 2 was imposed for the comparison between distal and proximal regions. A final requirement was that middle samples had to exhibit RPKM values mid-way between proximal and distal regions to selectively capture transcripts with a gradient between the two ends. **(C)** Affymetrix array data showing the differential expression of mRNAs encoding enzymes that regulate NADPH-production. Data was analysed to show fold change in expression of each transcript at the proximal compared to the distal region of the BP at E14. Microarray signals were normalized using the RMA algorithm. The mRNAs expressed at significantly different levels in distal versus proximal BP were selected based on ANOVA analysis by Partek Genomics Suite software (Partek, St. Charles, MO, USA) ***** $p < 0.05$.
ALDH1A3 - Aldehyde Dehydrogenase 1 Family Member A3, GOT2 - Glutamic-Oxaloacetic Transaminase 2, LDHB – Lactate dehydrogenase beta, PFKFB4 - 6-Phosphofructo-2-Kinase/Fructose-2,6-Biphosphatase 4, PKM2 – Pyruvate kinase M2, LDHA – Lactate dehydrogenase alpha, NNT - Nicotinamide Nucleotide Transhydrogenase, IDH3B – Isocitrate dehydrogenase beta, IDH3A - Isocitrate dehydrogenase alpha.

regulate NADPH-producing pathways (Figure 3). The largest contributor of cytosolic NADPH is the oxidative branch of the pentose phosphate pathway (PPP) [23]. NADPH can also be generated from mitochondrial tricarboxylic acid (TCA) cycle activity, where levels are maintained through the activity of multiple enzymes [23,24]. Although the specific mRNAs expressed at E6.5 and E14 differ, at both stages, metabolic genes with the highest differential expression between proximal and distal regions were associated with diversion of glucose into the PPP or towards aerobic respiration in mitochondria (Figure 3A, B). These expression data therefore reflect differences in NADPH-linked metabolism along the BP and are consistent with the higher τ_{bound} reported for the proximal BP region (Figure 1).

Tonotopic expression of metabolic effector proteins.

Modulation of metabolic pathways is driven predominantly through post-translational modifications of metabolic effector proteins [25]. Isocitrate dehydrogenase 3 (IDH3) and Lactate dehydrogenase (LDH) have well-defined roles in regulating the switch between glycolytic and oxidative metabolism during Warburg-like reprogramming [25-28]. They also regulate metabolic flux in the mitochondrial TCA cycle and cytosolic glycolysis respectively (Figure 4A). Therefore, we analysed the expression of IDH3 subunit A and LDH subunit A along the tonotopic axis of the developing BP. There was no difference

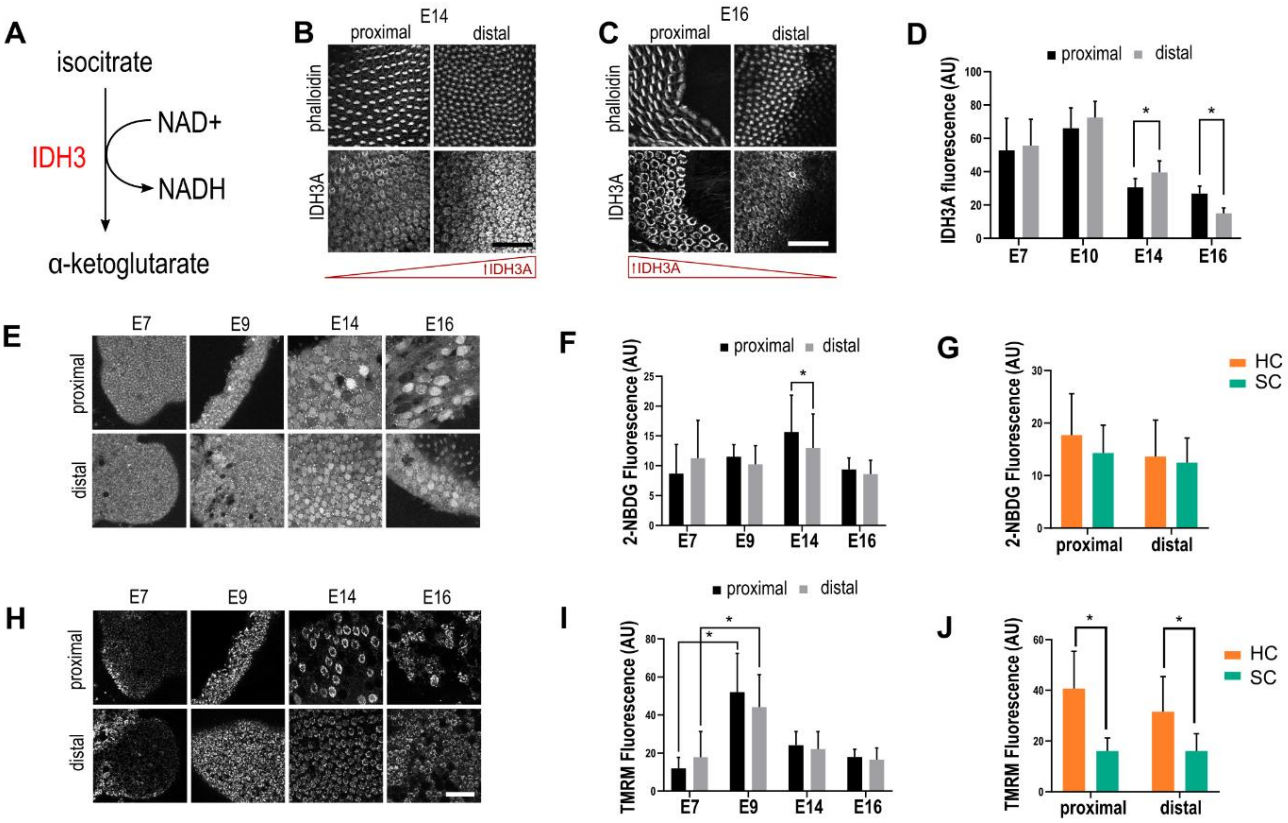

Figure 4. Glucose uptake and mitochondrial metabolism vary with developmental age, cell type and position along the tonotopic axis.

(A) Schematic showing IDH3 activity in the mitochondrial TCA cycle.

(B, C) Developmental expression of the mitochondrial TCA cycle enzyme IDH3A. Images show BP explants at E14 and E16 stained with Phalloidin, as a marker of filamentous Actin and labelled for IDH3 subunit A. Expression of IDH3A was significantly reduced at E14 compared to E7 and E10, both in proximal and distal regions. At E14 a distal-to-proximal gradient in IDH3A expression is established and by E16 this gradient is reversed along the BP.

(D) Quantification of IDH3A expression in proximal (black bars) and distal (grey bars) BP regions throughout development.

(E) 2-NBDG fluorescence in live BP explants shows no difference in glucose uptake along the proximal-to-distal axis or between cell types during development.

(F) Quantification of glucose uptake, as indicated by 2-NBDG fluorescence, in proximal (black bars) and distal (grey bars) BP regions between E7 and E14.

(G) Analysis of 2-NBDG fluorescence in hair cells and supporting cells at E14.

(H) Mitochondrial membrane potential measured (in the same cultures as in panel E) using TMRM fluorescence in single z-planes from image stacks in the proximal and distal regions of live BP explants.

(I) Quantification of TMRM fluorescence indicates a significant increase in mitochondrial activity between E7 and E9, followed by significant decrease between E9 and E14.

(J) TMRM fluorescence is significantly higher in hair cells compared to supporting cells in proximal and distal BP regions at E10 and E14.All data are represented as means ± SEM. For TMRM n = 6 biological replicates for E7, E10, E14. p = 0.04, and 0.002 Student's *t*-test. HCs vs SCs, proximal: n = 6 biological replicates, p = 0.035 and 0.039 for proximal and distal regions respectively, Student's *t*-test. IDH3A: E7 n=3, E10 n=3, E14 n=5 biological replicates. $P < 0.05$ Student's *t*-test. Scale bars = 40 μm.

in IDH3A expression between proximal and distal regions at early stages. However, between E14 and E16, the expression gradient of IDH3A reversed along the tonotopic axis (Figure 4B, C, Figure 4 supplement 1A). Downregulation of IDH3A has been linked specifically with a switch from oxidative to glycolytic pathways by reducing glucose flux in the mitochondrial TCA cycle [28]. The distal-to-proximal gradient in IDH3a expression at E14 (Figure 4B, D, Figure 4 supplement 1A) is consistent with a higher cytosolic glucose flux in the low frequency region of the BP. Alongside the higher NADPH/NADH ratio reported for the proximal BP (Figure 1) these findings are consistent with greater PPP activity in the low frequency region and progressively more oxidative metabolic phenotypes towards the distal region. The reversal in the IDH3A gradient at E16 (Figure 4C, D, Figure 4 supplement 1A) indicates a shift in metabolic function along the tonotopic axis as the system matures. Studies in other systems have shown that IDH3A regulates synaptic transmission by controlling vesicle fusion and recycling. Downregulation of IDH3A expression also phenocopies loss of the synaptic Ca^{2+} sensor synaptotagmin1 [29].

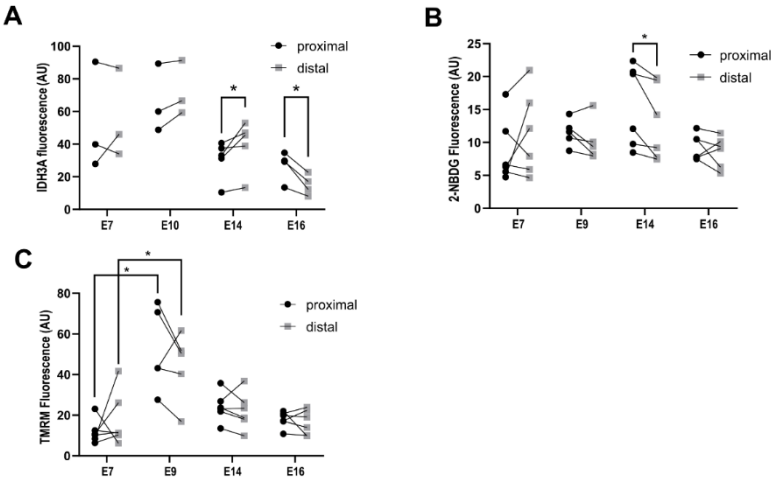

Figure 4 Supplement 1. Line graphs showing the trends in **(A)** IDH3A expression, **(B)** 2-NBDG and **(C)**TMRM fluorescence and along the proximal-to-distal axis of the developing BP. Data are mean ± SEM, $p < 0.05$, Student's *t*-test. n = 4 for IDH3A; n = 6 for 2-NBDG; n = 6 for TMRM.

The opposing gradient in IDH3A expression at E16 may therefore coincide with the functional refinement of hair cell synapses along the BP at this time. No difference in LDHA expression was seen between proximal and distal regions at any developmental stage. Instead, LDHA expression switched from SCs to HCs between E7 and E10 and was restricted to SCs again between E10 and E14 (Figure 4 supplement 2). The mechanisms regulating these cell-specific changes in LDHA expression are not known. The timing of these switches does however overlap with important stages in HC development. It will therefore be of interest to investigate potential crosstalk between LDHA-linked metabolism and the developmental pathways that instruct HC and SC specification.

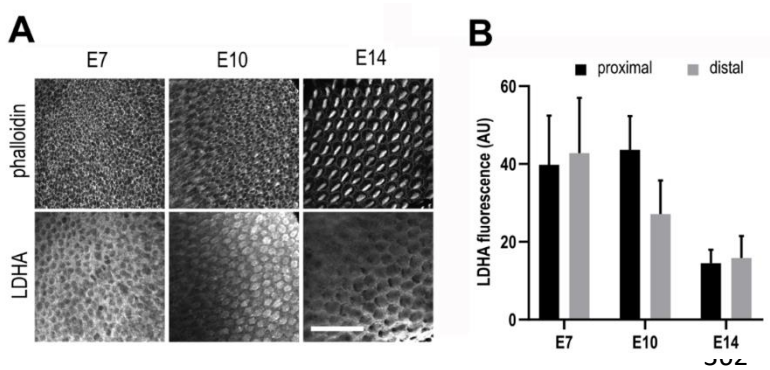

Figure 4 Supplement 2. Changes in the cell-specific expression of the glycolytic regulator LDHA during cochlear development.
(A) BP explants stained with Phalloidin and labelled for the metabolic enzyme LDHA. Phalloidin marks the hair cells at different stages of cochlear development (E7-E14). At E7, LDHA expression is localised to supporting cells. By E10 expression is restricted to the hair cells. **(B)** No differences in LDHA expression were evident along the proximal-to-distal axis of the BP at any developmental stage. Indicating a reprogramming of glucose metabolism, the expression of LDHA reduced significantly in the proximal (black bars) but not distal (grey bars) region at E14. Data are mean ± SEM. * $p < 0.05$ Student's *t*-test.

A gradient in glucose uptake is established along the tonotopic axis during BP development.

To further characterise differences in glucose metabolism along the tonotopic axis, we used the fluorescent D-glucose derivative 2-[N-(7-nitrobenz-2-oxa-1,3-diazol-4-yl)-amino]-2-deoxy-D-glucose (2-NBDG) [30] and the potentiometric fluorescent dye tetramethyl-rhodamine-methyl-ester (TMRM). The cellular fluorescence after incubation with 2-NBDG for 2 hours was used as an indicator of glucose uptake. TMRM was used to report mitochondrial membrane potential ($\Delta\Psi_{mt}$), itself a read-out of glycolytically-derived pyruvate oxidation in the mitochondrial tricarboxylic acid (TCA) cycle. Explants were dual-loaded with TMRM and 2-NBDG and fluorescence from both dyes was analysed from single cells in live BP explants between E7 and E16 (Figure 4E-J, Figure 4 supplement 1B, C). We observed no tonotopic difference in glucose uptake during early development or between HC and SC subtypes. A significant gradient in glucose uptake was evident however along the proximal-to-distal axis at E14 (Figure 4F). Measuring mitochondrial membrane potential using TMRM, from the same explants, revealed no significant difference in $\Delta\Psi_{mt}$ between proximal and distal end at any developmental stage. This indicates a uniform mitochondrial activity along the BP during development. Despite no differences along the tonotopic axis, $\Delta\Psi_{mt}$ did change significantly ($p < 0.05$ Student's *t*-test) with developmental age (Figure 4H-J, Figure 4 supplement 1C) reflecting a change in mitochondrial metabolism during HC formation at a stage when cells are becoming post mitotic [31] . The higher $\Delta\Psi_{mt}$ observed in HCs compared to SCs from E9 may reflect a unique metabolic state that develops in association with commitment to different cell lineages (Figure 4J). These findings also confirm that the gradient in NADPH/NADH (Figure 1D-I) along the BP originates specifically from tonotopic differences in cytosolic and not mitochondrial metabolism.

Cytosolic glucose metabolism is necessary for tonotopic patterning in the chick cochlea.

Having identified differential NADPH-linked glucose metabolism along the proximal-to-distal axis, we next investigated a functional role for this gradient in the establishment of tonotopy. Using 2-deoxy-d-glucose (2-DOG), to inhibit hexokinase (HK) activity, we blocked glycolysis during development [32]. BP explants were established at E6.5 and maintained for 7 days *in vitro* in control medium or that containing 2mM 2-DOG with 5mM sodium pyruvate (NaP), ensuring adequate substrate supply to the TCA cycle.

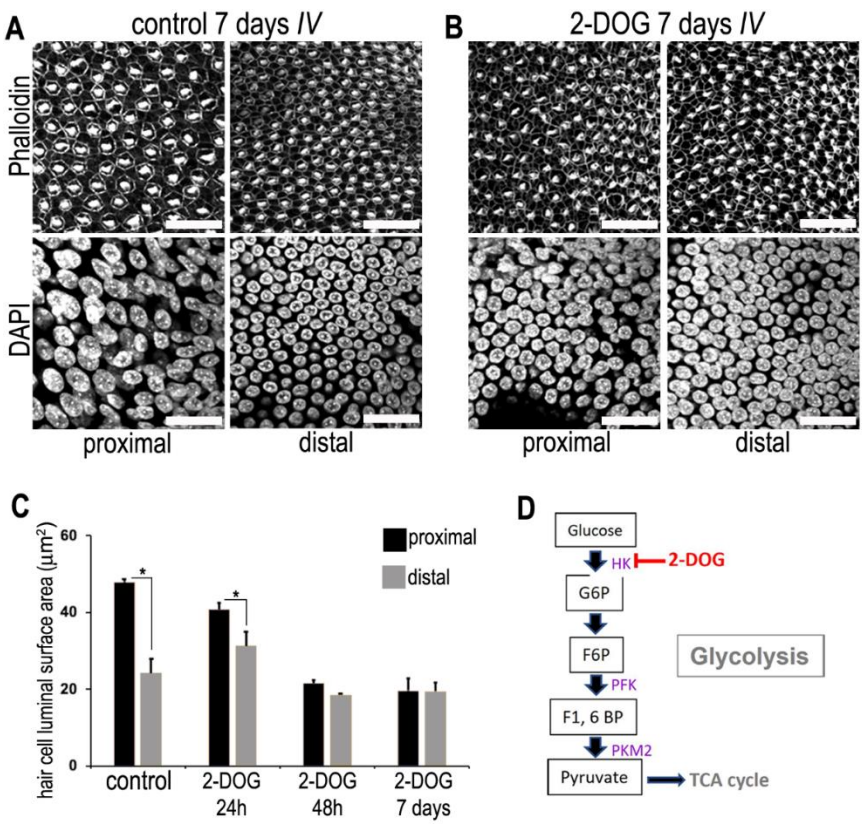

Figure 5. Blocking glycolysis at key stages of cochlear development induces distal-like phenotypes in the proximal BP.

(A-B) Maximum z-projections of BP explants showing Phalloidin and DAPI staining in the proximal and distal regions. Explants were maintained from E6.5 for 7 days *in vitro* (equivalent to E13.5) in either control medium or medium supplemented with 2mM 2-DOG + 5 mM Sodium Pyruvate (NaP). Phalloidin staining depicts differences in hair cell morphology between proximal and distal regions and DAPI indicates the gradient in hair cell size.

(C) Quantification of these differences**.** Hair cell luminal surface area was measured in 2500 μm^2 areas in the proximal (black bars) and distal (grey bars) BP regions for all culture conditions. In controls, mean hair cell luminal surface decreases progressively from the proximal-to-distal region. This gradient is abolished if glycolysis is blocked with 2-DOG between E6.5 and E13.5. 2-DOG caused a significant decrease in hair cell size in the proximal but not distal region. 2-DOG treatments were reduced to 24 or 48 hours to identify the developmental time window during which glycolysis takes effect. Following wash-out of 2-DOG after 24h, explants developed with normal hair cell positional identity and showed a significant decrease in luminal surface area along the proximal-to-distal axis. Explants treated with 2-DOG for 48 hours showed no recovery of positional identity following wash-out indicated by the loss of gradient in hair cell morphology.

(D) The target of 2-DOG inhibition.

Data are mean ± SEM. ***** $p < 0.05$ Student's paired *t*-test. Controls; n = 4, 2-DOG; n = 5, 24 2-DOG, n = 3 and 48h 2-DOG; n = 3 biological replicates. To ensure adequate substrate supply to the TCA cycle, 2-DOG-treated explants were supplemented with NaP. G6P glucose 6-phosphate, F6P – fructose 6-phosphate, F16BP – fructose 1,6-bisphosphate, 2-DOG – 2-deoxyglucose. Scale bars are 20 µm.

In a normal BP, hair cells are larger in the proximal than the distal region which can be determined morphologically using differences in the HC luminal surface area along the organ. This gradient is recapitulated in BP explant cultures [18]. In these experiments, HC luminal surface area, a morphometric that is tonotopically driven, was used as a read-out of HC size along the BP. The luminal surface area, measured using Phalloidin staining and HC density, estimated with DAPI, provided read-outs of HC phenotypes at different positions along the tonotopic axis (Figure 5 B, C). In control cultures, HCs developed with the normal tonotopic gradient in morphologies (luminal surface area and density)

(Figure 5A, C). In contrast, when glycolysis was blocked between E6.5 and E13.5 equivalent, tonotopic patterning was not just abolished, HC phenotypes appeared flattened and uniformly more distal-like along the BP. To further confirm a role for glycolysis in establishing positional identity, we employed a second method to modulate glucose metabolism. Studies in other systems have shown that raising cytosolic levels of the metabolite s-adenosyl methionine (SAM) blocks glycolysis independently of HK activity [33]. As seen in treatments with 2-DOG, tonotopic patterning was flattened in explants cultured with medium containing 50 μM SAM (Figure 5 supplement 1).

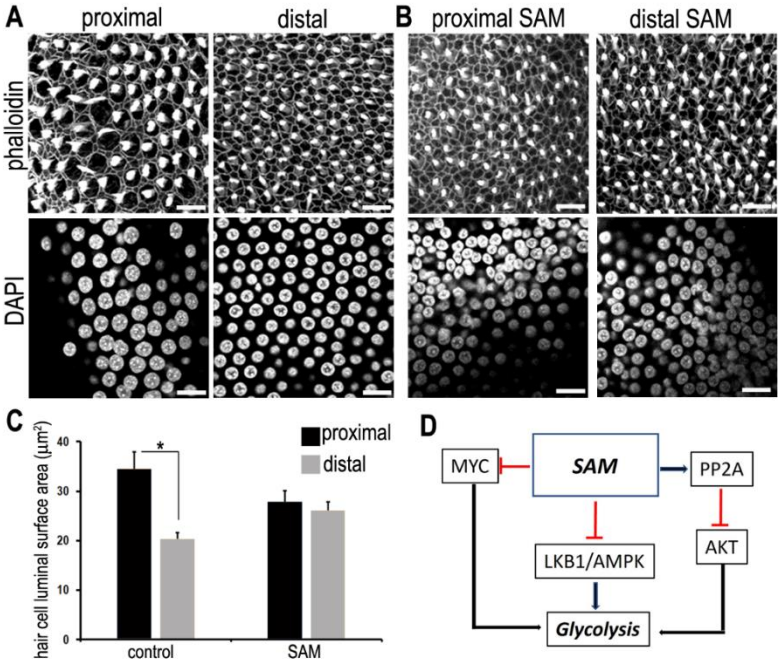

Figure 5 Supplement 1. Modulating S-Adenosyl methionine during development abolishes the gradient in hair cell morphology along the tonotopic axis of the BP.
(A-B) Images are maximal z-projections of proximal and distal regions from BP explants maintained for 7 days *in vitro* in control medium or medium containing 50 μM SAM. Phalloidin staining (A, B top panels) shows the BP surface and hair cell luminal surface areas and DAPI staining (A, B bottom panels) shows the hair cell size and density along the proximal-to-distal axis.
(C) Treatment of explants with SAM from E6.5 for 7 days *in vitro* abolished the normal gradient in hair luminal surface area along the tonotopic axis. This effect was most pronounced in the proximal compared to distal region. Hair cell luminal surface areas were measured from 2500 μm^2 areas in the proximal (black bars) and distal (grey bars) BP regions of control and SAM-treated explants.
(D) Schematic showing how increasing SAM levels indirectly modulates glycolytic flux.
Data are mean ± SEM. * $p < 0.05$ Student's paired *t*-test. Controls: n = 5 and SAM: n = 4 biological replicates. Scale bars are 20 μm. MYC - MYC Proto-Oncogene, BHLH Transcription Factor, SAM - S-Adenosyl methionine, PP2A – protein phosphatase 2, AKT - *Akt* serine/threonine kinase family, LKB1/AMPK – serine threonine kinase pathway in volved in metabolic regulation.

A distal-to-proximal gradient of Bmp7 activity is known to establish tonotopy in the BP between E6 and E8 [18]. To determine whether glucose metabolism acts during this same developmental window, we treated explants with 2-DOG for defined periods during HC formation. BPs were established at E6.5 and treated with 2-DOG for either 24 or 48 hours followed by wash out with control medium. The tonotopic gradient in HC size developed normally in BPs treated with 2-DOG for 24 hours followed by wash-out but was absent in those treated for 48 hours (Figure 5C). These results suggest that glucose metabolism acts during the same developmental time window as Bmp7, establishing the tonotopic gradient in HC size between E6 and E8.

Glycolysis, the PPP and pyruvate mediated OXPHOS have distinct roles in HC development.
Glucose metabolism encompasses aerobic glycolysis and the PPP in the cytosol and the TCA cycle in mitochondria, all of which are affected by treatment with 2-DOG. Recent studies in other systems have linked both the PPP and TCA cycle with cell fate decisions during development and differentiation

[8,34]. We therefore sought to further dissect the glycolytic signalling network during specification of tonotopy in the developing BP. To investigate a role for PPP-linked glucose metabolism, BP explants were established as described, and treated with 50 μM 6 Aminonicotinamide (6-AN) between E6.5 and E13.5 equivalent.

Figure 6. Glycolytic flux through the pentose phosphate pathway modulates hair cell development and positional identity along the tonotopic axis of the BP.

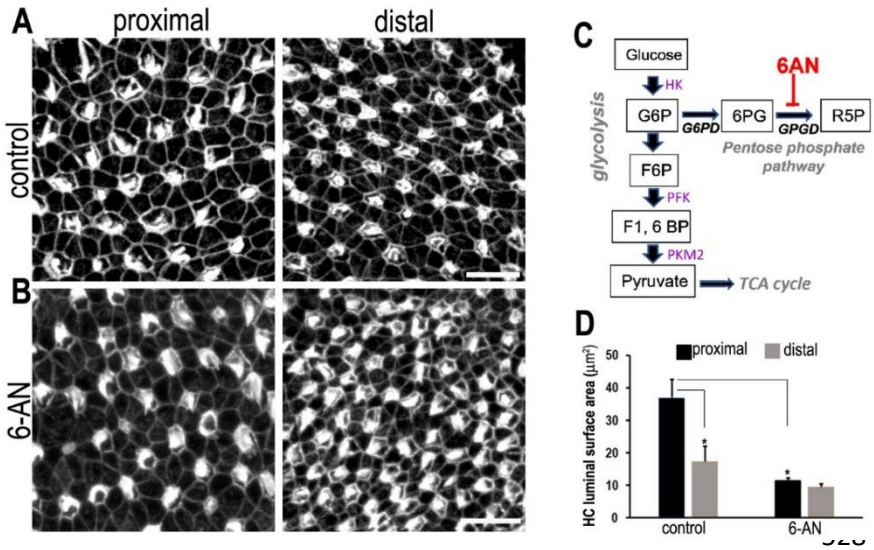

(A-B) Maximal z-projections of BP explants cultured from E6.5 for 7 days *in vitro* with control medium or medium containing 2 μM 6-AN. Images show the epithelial surface in proximal and distal BP regions stained with Phalloidin. **(C)**Treatment of explants with 6-AN, a specific blocker of glycolytic flux through the pentose phosphate pathway, caused a significant reduction in proximal compared to distal hair cell luminal surface area. **(D)** Quantification of hair cell size using measurement of the cuticular plate in defined 2500^2 μm areas in the proximal (black bars) and distal (grey bars) BP regions. Hair cell luminal surface area was quantified using Phalloidin staining. Data are mean ± SEM. * $p < 0.05$ Student's paired *t*-test. Controls: n = 5, 6-AN: n = 6 biological replicates. Scale bars are 10μm. G6P – glucose 6-phosphate, F6P – fructose 6-phosphate, F16BP – fructose 1,6-bisphosphate.

Treatment with 6-AN inhibits the rate-limiting PPP enzyme glucose-6-phosphate dehydrogenase (G6PD) (Figure 6C). By comparison with control cultures, inhibition of PPP metabolism caused a significant decrease in hair cell size within 2500 μm^2 areas measured in the proximal BP (Figure 6). To determine whether this effect was specific to glucose flux through the PPP we also blocked phosphofrucktokinase (PFK), a rate limiting enzyme further down in the glycolytic pathway, using 1μM YZ9 (supplementary Figure 4). Blocking PFK activity inhibits the glycolytic cascade involved in pyruvate production but does not change the activity of G6PD in the PPP [8]. Although we observed a reduction in HC size in both BP regions, inhibition of PFK between E6.5 and E13.5 did not alter the intrinsic tonotopic patterning in HCs along the axis of the epithelium ($p = 0.01$ Student's *t*-test proximal verses distal HC size) (Figure 6 supplement 1). These findings suggest that tonotopic patterning and specification of HC positional identity are regulated by metabolic glucose flux occurring upstream of PFK.

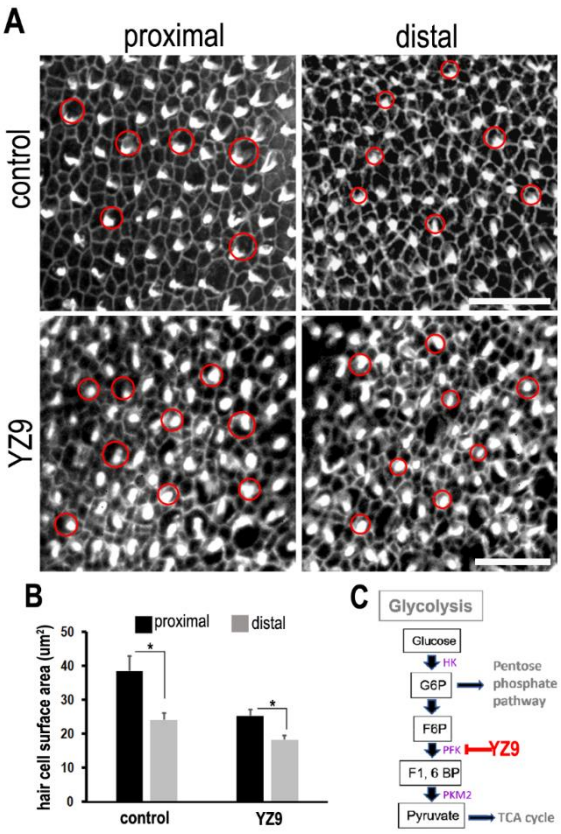

Figure 6 Supplement 1. Inhibiting phosphofructokinase has no effect on hair cell positional identity in the developing BP.
(A) Maximal z-projections showing Phalloidin staining in proximal and distal BP regions of control and YZ9-treated explants.
(B) Blocking glycolysis at the level of PFK between E6.5 and E13.5 had no effect on hair cell morphology along the tonotopic axis. Hair cell circumference was quantified in 2500 μm^2 areas in proximal (blue bars) and distal (orange bars) regions, showing no difference in size or density after treatment with 1μM YZ9.
(C) Schematic illustrating the inhibitory action of YZ9 in the glycolytic pathway.
Data are mean ± SEM. * $p < 0.05$ Student's paired *t*-test. Controls: n = 4, YZ9: n = 3. Scale bars are 20 μm. Red circles indicate size hair cell luminal surface area between control and YZ9-treated explants. G6P – glucose 6-phosphate, F6P – fructose 6-phosphate, F1, 6BP – fructose 1,6-bisphosphate.

Opposing gradients of glucose metabolism and mitochondrial OXPHOS have been described in developing chick embryos, where they regulate elongation of the body axis and specification of cell fates [9]. To investigate a role for the mitochondrial TCA cycle and thus OXPHOS along the tonotopic axis, we blocked the mitochondrial pyruvate carrier (MPC) using UK5099 (Figure 7B). [35] Preventing pyruvate uptake into mitochondria inhibits the TCA cycle and, as a result, impairs OXPHOS (Figure 7). HCs in explants treated with UK5099 between E6.5 and E13.5 did not develop with normal gradients in HC size along the BP and had either immature stereocilial bundles or lacked them completely in both proximal and distal regions (Figure 7A, C, red arrows). To determine whether this effect was due to an overall arrest in HC development, explants were established at E8.5, by which time positional identity is specified but bundles are not yet developed and maintained for 7 days *in vitro* to the equivalent of E15.5. Compared to control explants, those treated with UK5099 displayed no tonotopic gradient in cell size and HCs at all positions along the BP showed immature bundle morphologies (Figure 7C). Together, these findings suggest that mitochondrial TCA cycle activity and OXPHOS are necessary for the overall progression of HC maturation. The role of these pathways in establishing tonotopy is at present unclear and requires further investigation.

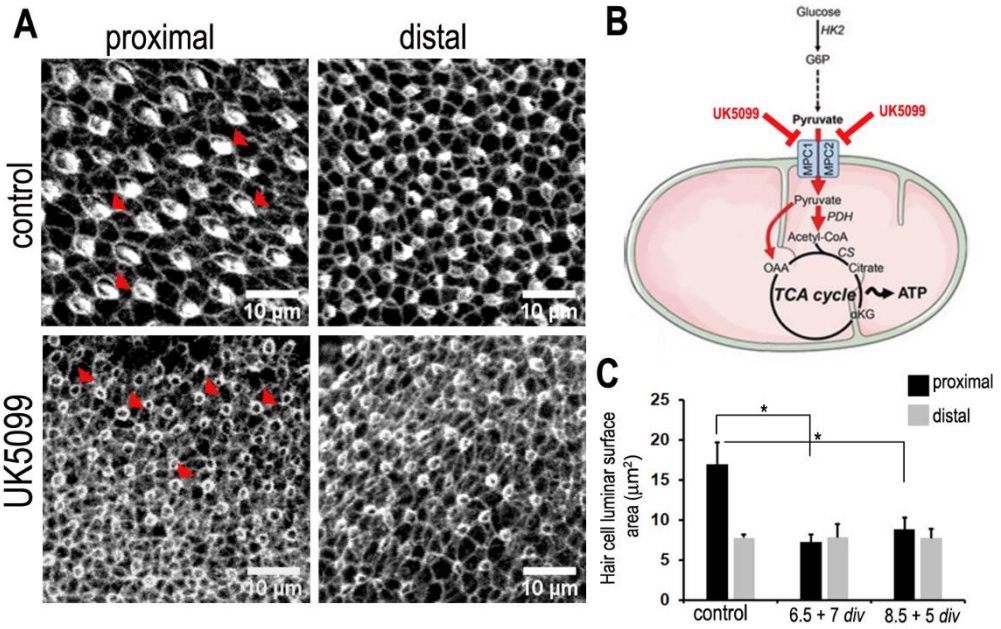

Figure 7. Mitochondrial OXPHOS is necessary for the normal developmental progression of hair cells but not positional identity.

(A) Hair cell morphology at the surface of the BP epithelium in explants stained with Phalloidin. Cultures were established at E6.5 and maintained for 7 days *in vitro* in control medium of that supplemented with the mitochondrial inhibitor UK5099.

(B) Blocking pyruvate uptake into mitochondria with UK5099 disrupts normal TCA cycle activity and thus mitochondrial OXPHOS by blocking uptake of pyruvate through the mitochondrial pyruvate carrier (MPC1/MPC2).

(C) Blocking mitochondrial metabolism Between E6.5 and E13 resulted in developmental abnormalities in HCs along the BP and a significant reduction in hair cell size in the proximal region. Stereocilia bundles of hair cells in the proximal BP region (red arrows) appeared immature compared to controls and those at the distal end. To determine whether mitochondrial OXPHOS acts during a specific developmental time window, cultures were treated with 1µM UK5099 for 7 days *in vitro* from E6.5 or for 5 days *in vitro* from E8.5. These times points are both be equivalent developmentally to E13.5. for Proximal hair cells showed no recovery following UK5099 wash-out. Data are mean ± SEM. * $p < 0.05$, Student's *t*-test.

Glucose metabolism regulates tonotopic expression of Bmp7 and Chdl-1

In many developing systems, gradients of one or more morphogen act to regulate cell fate, growth and patterning along a given axis [36,37]. In the chick cochlea, reciprocal gradients of Bmp7 and its antagonist Chdl-1 play key roles in determining positional identity. As disruption of both the normal gradient in Bmp7 activity [18] and glucose metabolism induce similar effects on tonotopic patterning (Figure 8A-C), we sought to investigate potential crosstalk between metabolism and known developmental signalling pathways that set up tonotopy. We investigated the regulatory effects of glucose metabolism on the expression gradients of Bmp7 and Chdl-1 along the developing BP. Explants were established at E6.5 and maintained for 72 hours *in vitro* (equivalent of E9.5) in control medium or that containing 2mM 2-DOG + 5mM sodium pyruvate.

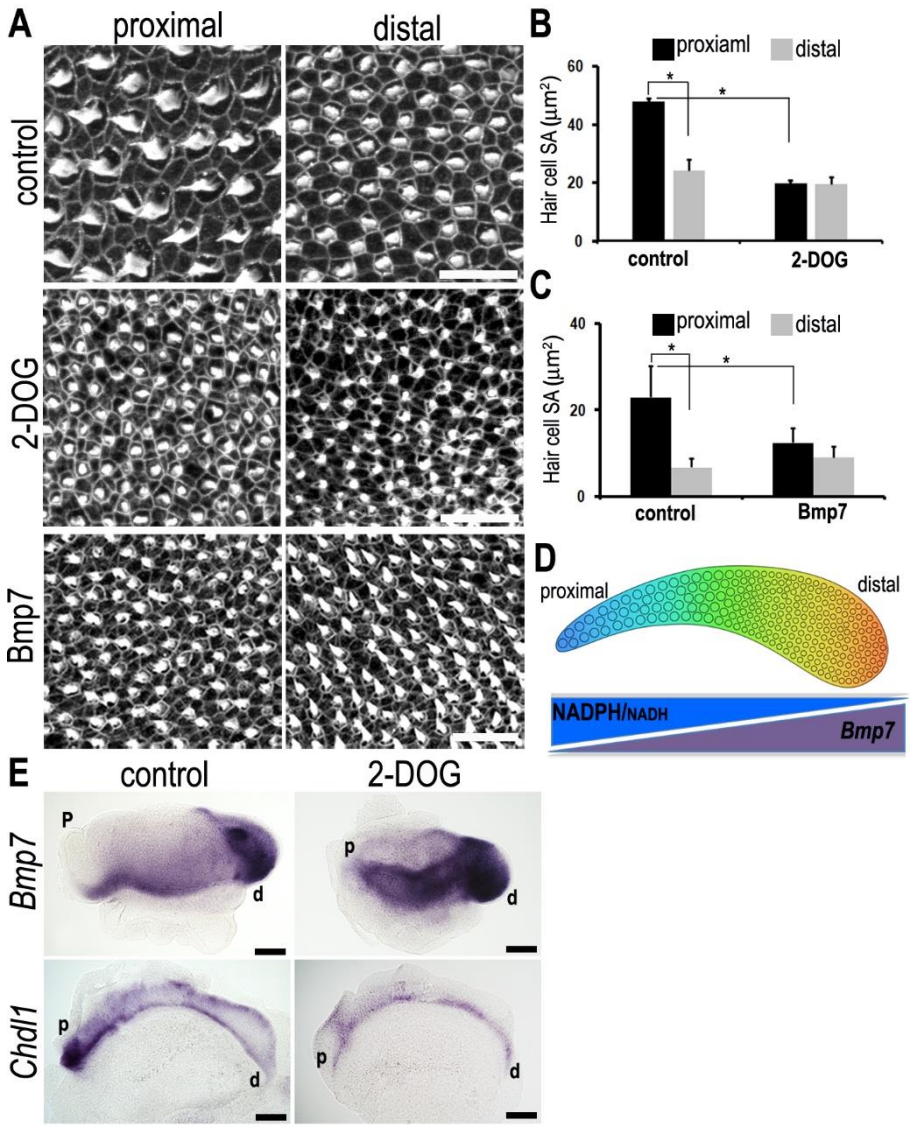

Figure 8. A tonotopic gradient in NAD(P)H producing glucose metabolism specifies hair cell positional identity along the BP by regulating gradients of Bmp7 and Chordin like-1.
(A) Phalloidin staining at the surface of BP explants in the proximal and distal regions. Explants were established at E6.5 and incubated for 7 days *in vitro* in control medium or medium containing 2-DOG + NaP or Bmp7.
(B-C) Treatment with 2-DOG or Bmp7 induced hair cell morphologies consistent with a more distal phenotype in the proximal BP. Hair cell luminal surface area was determined using Phalloidin staining at the cuticular plate in 2500^2 µm areas at both proximal and distal ends.
(D) Schematic of the chick BP, showing the graded differences in hair cell size and density along the tonotopic axis. The opposing gradients in Bmp7 activity and the cellular NAD(P)H/NADH ratio are indicated.
(E) Treatment of explant cultures with 2-DOG + NaP from E6.5 for 7 days *in vitro* disrupts the normal tonotopic expression gradients of Bmp7 and its antagonist Chordin like-1. Images show *in situ hybridisation* for *Bmp7* and *Chordin like-1* in BP whole-mounts treated with 2-DOG +NaP from E6.5 for 7 days *in vitro*. Note the disruption of both gradients when glycolysis is blocked during development. Controls: n=8, 2-DOG: n=6 Data mean ± SEM. * $p < 0.05$ Student's *t*-test. Scale bars (A) control, DOG are 20 µm and Bmp7 is 50 µm. Scale bars (E) are 10µm.

Disrupting glucose metabolism along the BP altered the normal expression gradients in both Bmp7 and Chdl-1 (Figure 8E). Specifically, following treatment with 2-DOG, the Bmp7 expression increased into the proximal BP region and expression of Chdl-1 decreased along the entire length of the organ. Equalised Bmp7 expression following treatment with 2-DOG caused expansion of HC phenotypes that more closely resembled distal differentiation into the proximal BP. Taken together, our findings

indicate a causal link between glycolysis and Bmp7 signalling in specifying HC identity along the tonotopic axis.

Changes in glucose metabolism do not alter proliferation in the BP

Changes in glucose metabolism have been linked with reduced cellular proliferation in other systems [38]. To determine whether the change in HC morphology observed in 2-DOG treated explants was a result of altered proliferation, the mitotic tracer EdU was added to cultures with 2-DOG for 72 hours. We observed no differences in proliferation in proximal or distal regions following treatment with 2-DOG + 5mM NaP (Figure 8 supplement 1).

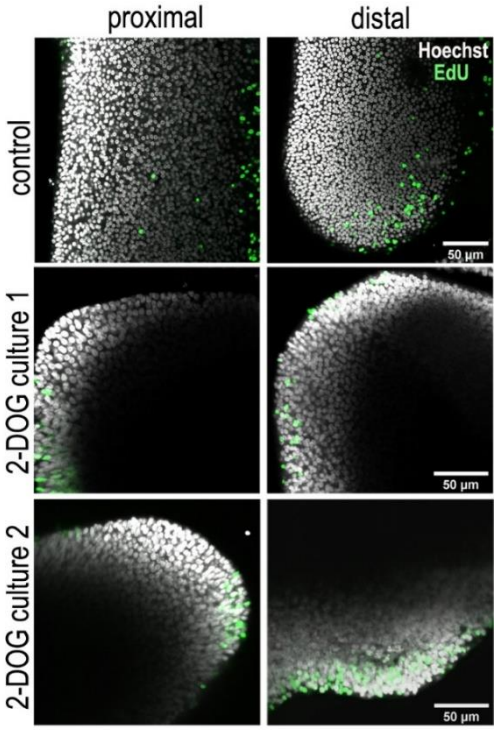

Figure 8 Supplement 1. 2-Deoxyglucose does not alter proliferation in the developing BP.
Images are maximal z-projections of the sensory epithelium in BP explants treated for 24 hours *in vitro* with either control (top) or 2-DOG + sodium pyruvate supplemented (bottom) medium. Cultures are stained with EdU (green) as a marker for proliferation and Hoechst to label cell nuclei (grey). Cultures were established at E7 and treated for 24 hours to *in vitro* capturing the period of active proliferation in the epithelium.

A role for NADPH-linked metabolism in the developing mouse cochlea

Unlike in the avian auditory system, HCs in the mammalian cochlea cannot spontaneously regenerate after damage [39]. Although we can generate new HCs using organoid models that recapitulate aspects of early inner development, cells produced using these methods are not functionally viable long-term and do not display all features of mature HCs [40]. Identifying novel factors and signalling pathways that regulate the specification and formation of HCs subtypes in the mammalian auditory system is therefore necessary. Metabolism has not been explored in developing HCs and SCs of the mammalian cochlea. We do know, however, that in the adult cochlea HCs and SCs have distinct metabolic states linked to their function [12]. We provide the first characterisation of metabolism in HCs and SCs in living explants of the developing mammalian cochlea. Cells were analysed between E14 and P0, the developmental window for cell fate specification and functional refinement. As observed in the chick cochlea, there was no difference in the NAD(P)H FLIM signal between HCs and SCs at early developmental stages. At later time points however, there was a significant ($p < 0.05$, Student's t-test) increase in τ_{bound} and α_{bound} between E14 and E16 indicating a metabolic shift (Figure 9A-F). The divergence in metabolic state between HCs and SCs during development (Figure 9D-F) suggests a possible link between metabolic reprogramming and the progression along distinct cell lineages. Similar metabolic reprogramming has been described in differentiating cell types of other complex tissues [5,41].

To investigate the biochemistry underlying metabolic differences between HC and SC sub-types, we interrogated existing single cell datasets derived across 3 developmental time points from the mouse cochlea [42]. HCs were identified using expression of *Pou4f3* and lack of *Sox2* [42,43]. Conversely, SCs were identified using expression of *Sox2* [42,44]. We then performed a comparative analysis using the Seurat (v4) package, in R [45,46]. As discussed, an increased τ_{bound} reflects a higher NADPH/NADH ratio, regulated mainly by the PPP activity in the cytosol. We therefore investigated expression of genes

730 encoding enzymes that regulate PPP metabolism. We found that PPP pathway regulatory enzymes are
731 more highly expressed in SCs compared to HCs at all developmental time points (Figure 9G). We
732 observed developmental changes in the expression of regulatory enzymes of NADPH metabolism.
733 Increased expression in cytosolic *Nadk*, (generates $NADP^+$ from NAD), in HCs between E14 and E16
734 (Figure 9G) likely corresponds to the higher anabolic activity associated with differentiation along the
735 cochlea at this time and thus the greater requirement for PPP-derived NADPH [47]. Additionally at the
736 same time points, we detected a pronounced upregulation in *Pgls,* a major regulator of the PPP and
737 of ribose-5-phosphate production [48]. Heightened availability of this enzyme would provide the
738 necessary biosynthetic precursors for nucleic acid synthesis during cell differentiation [48]. We also
739 investigated differences in the expression of genes encoding regulators of mitochondrial NADPH
740 production (Figure 9H). We observed that expression of mitochondrial NADPH-producing enzymes is
741 similar between E14 and E16 in both HCs and SCs but becomes restricted to HCs by P1. This likely
742 reflects progressive commitment along the HC lineage, which we know is associated with enhanced
743 mitochondrial activity [42].

744 **Discussion**

745 To successfully address hearing and balance defects, we must be able to generate new, functionally
746 viable HCs following damage, aging or ototoxic insult. Additionally, as high frequency HCs are more
747 vulnerable to insult, it is essential we understand the specific factors that specify different HC subtypes
748 along the tonotopic axis. Generating new HCs that recapitulate the features of those in a healthy
749 cochlea requires a detailed knowledge of the cell biology and signalling that drives their formation.
750 Further to this, it is important we resolve how they navigate the path of maturation and survival within
751 their surrounding niche along the cochlea. Previous studies have focused largely on understanding the
752 role of transcription factors in HC formation and how manipulation of these in the adult inner ear can
753 be exploited to promote regeneration [43,49-52]. Taking a novel approach, we here explored the
754 coordinated regulation of complex signalling between developmental pathways and metabolism in
755 differentiating HCs and SCs of the inner ear.
756
757 Using FLIM imaging of cellular NAD(P)H, we observed a proximal-to-distal gradient in glucose
758 metabolism in the developing BP resulting from tonotopic differences in PPP activity. We confirm this
759 gradient using bulk RNA-seq and Affymetrix microarray data, which identified tonotopic expression of
760 mRNAs encoding PPP regulatory enzymes (GOT2 [53], PKM2 [54], PFKFB4 [55,56]). High levels of NADPH
761 generated through PPP-linked metabolism have been reported in proliferating cells during
762 development and differentiation in a number of systems where they regulate cell cycle progression
763 and cell size [57,58]. Graded differences in cell size along the cochlea are important for correct tonotopy
764 and hearing. Cell size is determined by two opposing processes, growth and division [59] and PPP activity
765 is known to regulate the signalling pathways that coordinate these [60]. The mechanisms linking cell
766 growth, cell cycle progression and cell size regulation are poorly understood in the context of intact
767 tissues such as the cochlea. In the BP, cell cycle exit is initiated in the distal region at embryonic day 5
768 (E5). Terminal mitosis then progresses in a wave from distal-to-proximal regions and across the neural-
769 to-abneural axis until E9, when the majority of cells are postmitotic [31]. As critical cell size and cell cycle
770 progression are determined by environmental factors, one hypothesis is that by differentially
771 regulating growth along the BP and thus timing of cell cycle exit, the gradient in glycolysis could
772 instruct tonotopic differences in HC cell size.

773
774

775

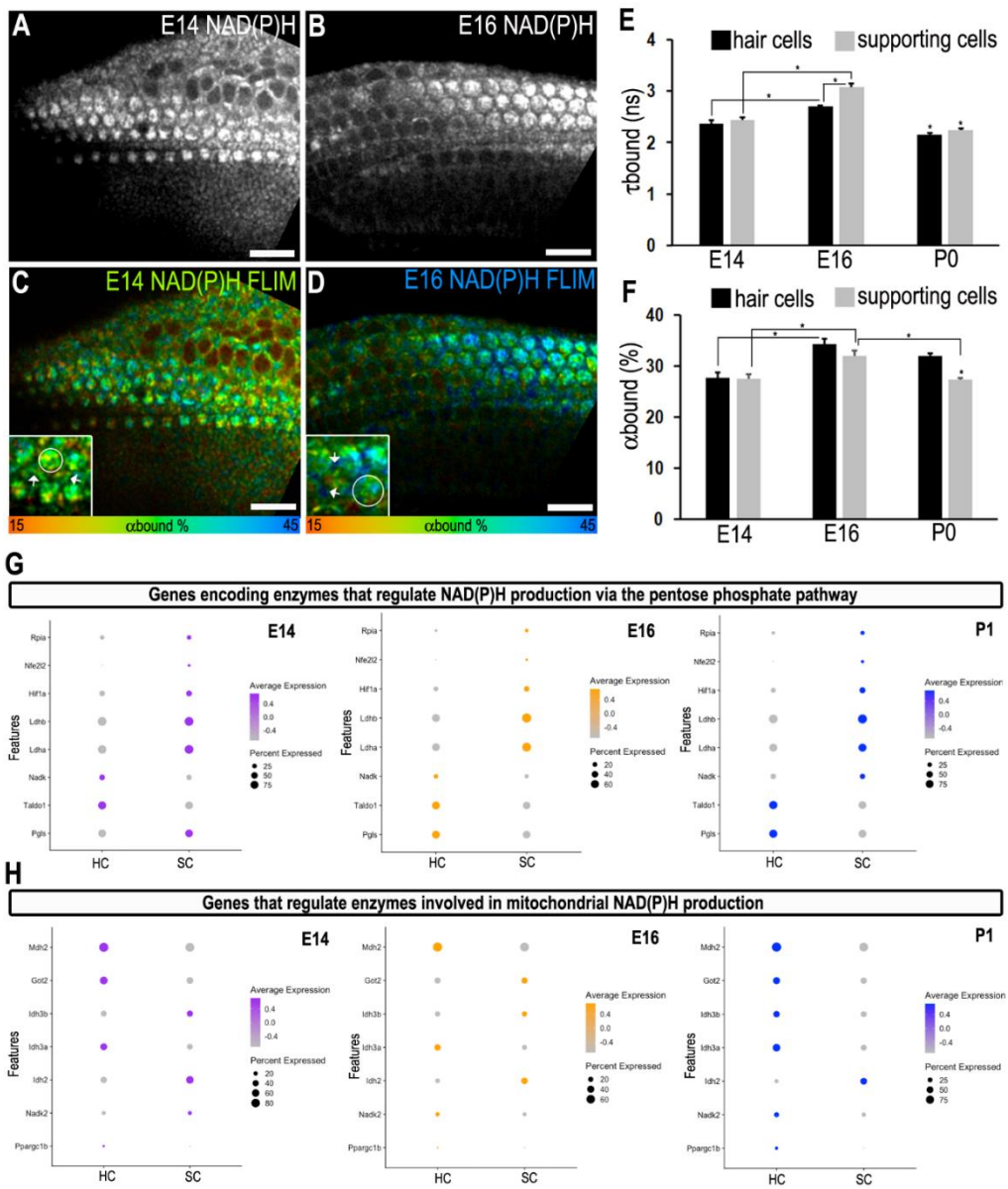

Figure 9. Hair cells and supporting cells in the mammalian cochlea show differential expression of genes regulating cellular NADPH/NADH.

(A-B) NAD(P)H fluorescence in live cochlear explants at E14 and E16.

(C-D) NAD(P)H lifetime images extracted for α_{bound} at E14 and E16. Differences in α_{bound} show switching between glycolytic and oxidative metabolism during cochlear development. Insets highlight differences in α_{bound} and thus metabolism between HCs (black bars) and SCs (grey bars) at E16 but not E14. White arrows indicate the SCs and white circles outline the HCs.

(E) τ_{bound} increases in both HCs (black bars) and SCs (grey bars) between E14 and E16 and decrease significantly in both cell types between E16 and P0**.** The change in τ_{bound} indicates a shift in the cellular NADPH/NADH balance as a function of development. At E16, τ_{bound} is significantly higher in SCs (grey bars) compared to HCs (black bars) showing metabolic divergence between cell types as a function of development.

(F) α_{bound}**,** reflects the proportion of cellular NAD(P)H that is bound to either enzymes or cofactors and the balance between glycolysis and OXPHOS. α_{bound} increases significantly in both hair cells and supporting cells between E14 and E16 but decreases significantly in supporting cells only between E16 and P0**.** This indicates a reprogramming of metabolic pathways both developmentally and between cell types. Data are mean ± SEM. * $p < 0.05$ Student's paired *t*-test. E14: n = 3, E16: n = 5 and P0, n = 5 biological replicates. Scale bars are 50 µm.

(G-F) Dot plot visualisation of genes encoding key enzymes that regulate cellular levels of NAD(P)H across HCs and SCs at different stages of murine cochlea development. Size of dots encodes percentage of cells expressing

the named gene, while colour encodes the average expression of that genes across the cells within each group. Genes shown are for NAD(P)H regulation via the pentose phosphate pathway (G) or in the mitochondria (F).

By diverting glucose towards the PPP, nascent HCs within the epithelium would be exposed to lower levels of mitochondrially-derived reactive oxygen species (ROS) thus protecting newly synthesised DNA from ROS-induced damage during cell division. Enhanced PPP activity and increased NADPH levels during HC formation could therefore act to poise cells for the increased anabolic activity associated with differentiation and DNA synthesis [57]. At E9, the time at which cells become post mitotic, we also see a significant increase in mitochondrial metabolism reported by a more polarised membrane potential. This, in combination with the switch in IDH3A expression along the tonotopic axis between E14 and E16, indicates an extensive reprogramming of mitochondrial metabolism in association HC differentiation.

Morphogen signalling gradients have well defined roles in directing cell identity along developing axes, where distinct cell subtypes are determined as a function of morphogen concentration at different positions along them [36,61,62]. We show a gradient in glucose metabolism along the proximal-to-distal axis of the developing BP that regulates the morphological properties associated with tonotopic identity in HCs. Disruption of this gradient mimics the effects of altered Shh/Bmp/Chordin signalling [18,63], inducing distal-like HC phenotypes in the proximal BP region. Our findings therefore indicate a causal link between developmental and metabolic pathways along the cochlea during HC formation. The mechanisms underlying tonotopy in mammals differ from those in birds and lower vertebrates, however gradients in both Bmp7 and Shh are evident along the auditory organ in both systems during development [63]. We also know that Sonic Hedgehog (Shh) signalling positively regulates Bmp7 expression in the developing BP and regional identity in the developing mouse cochlea [63]and that their downstream targets differ between species. A role for glucose metabolism has not been explored in the mammalian cochlea, but it would be of significant value to determine potential crosstalk between graded metabolism and developmental pathways during HC formation in the mammalian inner ear.

In cells of the presomitic mesoderm, metabolism regulates morphogen signalling such that opposing gradients in glycolytic and oxidative pathways drive elongation of the body axis. Here, glycolysis acts to generate a gradient in intracellular pH (pHi), which in turn, modulates the activity of FGF and Wnt signalling pathways along the developing body axis [9-11]. Differences in pHi along the body axis determine neuronal and mesodermal cell fate by modulating the acetylation and thus stability of beta catenin [9]. Given the importance of Wnt signalling in cochlear development and HC formation, it would be of interest to determine whether the gradient in glucose metabolism along the developing BP establishes tonotopic differences in pHi and beta catenin acetylation. In the developing drosophila wing, impaired glycolysis upregulation Hedgehog (Hh) signalling by stabilising the membrane protein Smoothened at the primary cilia, but does not alter the normal levels or the expression pattern of Shh protein within the tissue [64]. The distalisation of HCs in the proximal BP region following 2-DOG treatment, may therefore be a consequence of increased Shh activity, which as a consequence enhances Bmp7 signalling. Investigating a regulatory role for glucose metabolism in the Shh-Bmp7-Chdl-1 signalling network along the proximal-to-distal axis of the chick cochlea and Shh signalling along the basal-to-apical axis in the mouse will further our current understanding of HC formation. Untangling the precise interactions between components of the Sonic Hedgehog-Bmp7-Retinoic acid and glycolytic signalling networks will further our knowledge of how hair cells could be tuned morphologically during their formation. From what we understand about frequency selectivity in vertebrates [65], recapitulation of tonotopy will also require that any gradients and the signalling networks they instruct, scale correctly in different inner ear sensory patches and across species with

879 varying head size and cochlear lengths. It will be important to understand how the molecular
880 mechanisms that link metabolic and developmental pathways during HC scale within different inner
881 ear sensory patches and across species.
882
883 Developmental programming of energy balance within HC and SC lineages is an important
884 physiological process allowing cells arising from a common progenitor population to differentiate with
885 unique metabolic states. Extensive changes in cellular redox state occur during the first postnatal week
886 of functional refinement in cells of the mouse cochlea [12,13]. These changes indicate local metabolic
887 switches during the early phases of HC and SC functional maturation [12]. We report cell-specific
888 differences in metabolic enzyme expression, NAD(P)H FLIM signatures and mitochondrial activity in
889 the cochlear epithelium from as early as E14 in mouse and E9 in chick. These cell-specific differences
890 may reflect the developmental origins of metabolic coupling between HCs and SCs. Such cooperation
891 is observed between neurons and astrocytes in the developing brain[66]. Neurons and astrocytes
892 preferentially use different metabolic pathways under physiological conditions, due in part, to cell
893 specific expression patterns of genes regulating energy metabolism [72]. Metabolic coupling is essential
894 for normal brain function and has also been linked with long-term function and survival of cochlear
895 hair cells [67,68]. Long-term hair cell function is not possible without auxilliary input from supporting cell
896 neigbours. Understanding the developmental programs and specific factors that determine future HC-
897 SC coupling within the cochlear niche is essential if we are to recapitulate such mechanisms and
898 sustain long-term HC viability in regenerative or organoid models.
899
900 **Materials and Methods**
901 **Embryo care and procedures**
902 Fertilized White Leghorn chicken (*gallus gallus domesticus*) eggs (Henry Stewart & Co. LTD, UK)) were
903 incubated at 37.5°C in an automatic rocking incubator (Brinsea®) until use at specific developmental
904 stages between E6 and E16. Embryos were removed from their eggs, staged according to Hamburger
905 and Hamilton (1951) and subsequently decapitated. All embryos were terminated prior to hatching at
906 E21. All procedures were performed in accord with United Kingdom legislation outlined in the Animals
907 (Scientific Procedures) Act 1986.
908
909 **Preparation of BP and cochleae explants for live imaging studies**
910 Mouse embryos were collected from timed-pregnant females, and cochlear explants were established
911 at E13 to E16 as previously described [69]. For live imaging, the most apical turn of the cochlear duct was
912 removed prior to culturing. Briefly, auditory bullae were removed and transferred into chilled L-15
913 medium (Life Technologies). The wall of the bulla was opened and the whole cochlea extracted. The
914 stria vascularis and Reissner's membrane were removed. All mice were maintained and handled in
915 accord with United Kingdom legislation outlined in the Animals (Scientific Procedures) Act 1986.
916 Explants were placed onto Millicell cell culture inserts (Millipore ®) and incubated overnight at 37°C.
917 Cochlear explants were maintained in Dulbecco's Modified Eagle medium F-12 (DMEM/F-12) and BP
918 explants in medium 199 Earl's salts (M199) (GIBCO, Invitrogen) both containing 2% fetal bovine serum
919 and 5 mM HEPES buffer (Life Technologies). For live imaging experiments explants were transferred
920 to glass-bottom 50 mm MatTek dishes and held in place using custom-made tissue harps (Scientifica).
921 Cultures were maintained in L-15 medium at room temperature throughout the experiment.
922
923 **Basilar papilla culture**
924 Basilar papillae (BPs) were isolated from embryos incubated for between 6 (E6.0) and 8 E8.0) days and
925 maintained in chilled Leibovitz's L-15 media (GIBCO, Invitrogen). Papillae were dissected as described

926 previously [70] and cultured nerve-side-down on Millicell cell culture inserts (Millipore ®). Cell culture
927 inserts were placed into 35 mm culture dishes containing 1.5 mL of medium 199 Earl's salts (M199)
928 (GIBCO, Invitrogen) supplemented with 5 mM HEPES buffer and 2% fetal bovine serum (FBS). Papillae
929 were maintained in M199 medium plus vehicle (control media) for up to 7 DIV until the equivalent of
930 embryonic day 13.5 (E13.5). For all treatments, a minimum of four samples were analysed. The
931 following factors were applied to experimental BPs in culture at the specified concentrations: 2-
932 Deoxyglucose (2-DOG) 2mM (SIGMA), Sodium Pyruvate (NaP) 5mM (SIGMA), 6-Aminonicotinamide
933 (6AN) 2μM (SIGMA), *S*-(5'-Adenosyl)-*L*-methionine chloride dihydrochloride (SAM) 50μM (SIGMA),
934 YZ9 1μM (SIGMA). For 2-DOG wash-out experiments, cultures were treated for 24 or 48 hours
935 followed by wash out with control medium for the remainder of the experiment up to 7 days.
936 For paired controls, medium was also changed at 24 and 48 hours in culture. At the conclusion
937 of each experiment (7 days *in vitro*), cultures were fixed in 4% paraformaldehyde (PFA) for 20 minutes
938 at room temperature, washed thoroughly three times with 0.1 M phosphate buffered saline
939 (Invitrogen) and processed for immunohistochemistry.
940
941 **Fluorescence lifetime imaging**
942 NAD(P)H FLIM was performed on an upright LSM 510 microscope (Carl Zeiss) with a 1.0 NA 40x water-
943 dipping objective using a 650-nm short-pass dichroic and 460±25 nm emission filter. Two-photon
944 excitation was provided by a Chameleon (Coherent) Ti:sapphire laser tuned to 720 nm, with on-sample
945 powers kept below 10 mW. Photon emission events were registered by an external detector (HPM-
946 100, Becker & Hickl) attached to a commercial time-correlated single photon counting electronics
947 module (SPC-830, Becker & Hickl) contained on a PCI board in a desktop computer. Scanning was
948 performed continuously for 2 min with a pixel dwell time of 1.6μs. Cells and position within the
949 epithelium was determined prior to FLIM analysis using the mitochondrially targeted fluorescent dye
950 tetramethylrhodamine methyl ester (TMRM). The dye was added to the recording medium, at a final
951 concentration of 350 nM, 45 min before imaging. TMRM fluorescence was collected using a 610±30
952 nm emission filter. Excitation was provided at the same wavelength as NAD(P)H to avoid possible
953 chromatic aberration. The 585±15 nm emission spectrum of TMRM ensured its fluorescence did not
954 interfere with acquisition of the NAD(P)H FLIM images.
955
956 **FLIM data analysis**
957 Following 5 x 5 binning of photon counts at each pixel, fluorescence decay curves of the form [12],
958 $$I(t) = Z + I_0\left([1-\alpha_{\text{bound}}]e^{-t/\tau_{\text{free}}} + \alpha_{\text{bound}}e^{-t/\tau_{\text{bound}}}\right)$$
959
960 were fit to the FLIM images using iterative reconvolution in SPCImage (Becker & Hickl), where Z allows
961 for time-uncorrelated background noise. Matrices of the fit parameters τ_{free}, α_{bound} and τ_{bound} and the
962 total photons counted were at each pixel, were exported and analysed for hair cells and supporting
963 cells, and proximal and distal BP regions, using SPCImage and ImageJ software packages.
964
965 **2-NBDG and TMRM live imaging**
966 The auditory sensory epithelia were isolated from E7, E9, E14 and E16 chick embryos in chilled L-15
967 medium. BPs were subsequently incubated in 1mM solution of 2-NBDG (N13195, Thermo Fisher
968 Scientific) in L-15 medium at room temperature for 1 hour. The medium was then replaced with a
969 fresh solution of 1mM 2-NBDG and 350 nm TMRM (T668, Thermo Fisher Scientific) in L-15 and
970 incubated for a further hour at room temperature. Afterwards, epithelia were washed several times
971 with fresh medium containing 350 nM TMRM and were mounted in a 3.5 mm glass bottom MatTek

dish. 3D image stacks with an optical thickness of 1µm were captured using a Leica SP5 confocal microscope with an HCX PL APO 63×/1.3 GLYC CORR CS (21 °C) objective.

Immunohistochemistry

Inner ear tissue was collected at various developmental stages, fixed for 20 min to one hour in in 0.1 M phosphate buffered saline (PBS) containing 4% paraformaldehyde (PFA), and processed for whole-mounts immunohistochemistry. The auditory sensory epithelium was then fine dissected and permeabilized in PBS containing 0.3% Triton for 30 min before immunostaining using standard procedures. Samples were stained with primary antibodies for LDHA 1:75 (Genetex GTX101416) and IDH3A 1:75 (ab228596, Abcam) and Calbindin 1:50 (ab82812, Abcam). Antibody staining was visualized using secondary antibodies conjugated to either Alexa 488 or Alexa 546 (Invitrogen). Cultures were incubated with all secondary antibodies for 1 hour at room temperature 1:1000, washed thoroughly in 0.1 M PBS. Samples were then incubated for an additional hour with either Alexa Fluor-conjugated Phalloidin-546 (Invitrogen) to label filamentous actin and DAPI 1:1000 to label cell nuclei. Tissue samples were mounted using either Prolong Gold antifade reagent (Invitrogen). 3D image stacks of mounted samples were captured using a Leica SP5 confocal microscope with an HCX PL APO 63×/1.3 GLYC CORR CS (21 °C) objective.

EdU staining

Control or 2-DOG-treated cultures were incubated for 48 hours in 10 µM 5-ethynyl-2'-deoxyuridine (EdU) from embryonic day 6 (E6) to embryonic day 8 (E8). Cultures were subsequently fixed for 15 minutes in 4% PFA at room temperature and then washed in 0.1M PBS. Explants were then processed for EdU staining following the Click-iT® EdU 488 protocol (Thermo Fischer Scientific).

Image analysis

Analysis of z-stacks from IHC stains as well as 2-NBDG and TMRM live imaging experiments was carried out using the Fiji distribution of imageJ. For each sample, a z-plane 2 µm beneath the surface of the epithelium was chosen for further analysis. For each of these selected z-planes, a 100 µm x 100 µm region of interest (ROI) was chosen containing intact tissue in which all HCs were optimally orientated. Mean fluorescence intensity of the tissue was measured for ROIs at E7, E9 and E10 timepoints. At E14 and E16, HCs were manually segmented. HC labels were dilated by 3 µm, which provided selections which included both hair cells and their surrounding SCs. By subtracting the hair cell segmentation from the dilated label, we were thus able to measure the fluorescence intensity of whole HCs separately from their surrounding support cells in the 2-NBDG and LDHA data. A similar approach was adopted when measuring TMRM and IDH3A fluorescence intensity at E14 and E16. However, we noticed that signal was concentrated around the HC periphery. In order to ensure that the fluorescence intensity best reflected only the mitochondria and was not reduced by the low fluorescence from the centre of each HC, we measured mean fluorescence intensity only up to 2 µm from the cell membrane. Likewise, for TMRM and IDH3A data at E7 and E9, mitochondria were segmented using Fiji's auto-local thresholding (Niblack) prior to intensity measurements, to avoid a biased estimate of fluorescence intensity due to empty space surrounding each mitochondrion.

Analysis of hair cell morphology

Data were analysed offline using image J software. Hair cell luminal surface area and cell size were used as indices for HC morphology along the tonotopic axis. To determine the hair cell density, the luminal surfaces of hair cells and cell size, cultures were labelled with phalloidin and DAPI. Then, the number of hair cells in 50 µm × 50 µm regions of interest (2,500 μm^2 total area) located in the proximal and distal BP regions were determined. Proximal and distal regions were determined based a

calculation of the entire length of the BP or explant. In addition, counting ROIs were placed in the mid-region of the BP along the neural to abneural axis to avoid any confounding measurements due to radial differences between tall and short hair cells. For each sample, hair cells were counted in four separate ROIs for each position along the BP. Luminal surface areas were determined by measuring the circumference of individual hair cells at the level of the cuticular plate.

In situ hybridisation

Inner ear tissue was dissected and fixed in 4% PFA overnight at 4 °C. Tissue was subsequently washed three times for 30 min in 0.1 M PBS and subsequently dehydrated in methanol (25–100%). Tissue was stored at −20 °C until use. Immediately before the *in situ* protocol, tissue was rehydrated using a reverse methanol gradient (100–25%). Complimentary digoxigenin-labelled RNA probes for *Bmp7* were kindly provided by Doris Wu (NIDCD, NIH). *Chd-l1* was synthesised as described previously [18]. All *in situ* hybridization reactions were performed as described previously.

Analysis of single cell RNA-seq data sets

Single cell sequencing data was obtained from the study under accession number GSE137299 [42]. The code to process the data was previously shared by the corresponding authors of the above referenced study (https://github.com/kelleylab/cochlearSEscrnaseq). For the purposes of the current analysis, hair cells were extracted from the above dataset using expression of *Pou4f3* and lack of *Sox2* as a metric. This was done for all investigated time points. To identify supporting cells, we used expression of *Sox2* as a metric. The resulting cells were integrated as described in the results section. Briefly, 2000 variable features were identified per type of cell, per time point, and these were used as anchors for integrating the datasets. Gene expression values were then scaled, normalised, and following linear dimensionality reduction, used for cell clustering to project the cells onto a Uniform Manifold Approximation and Projection for Dimension Reduction (UMAP) plot. Genes of interest were then visualised using Dot Plots across the different time points.

Acknowledgements

The authors wish to thank Matthew Kelley, Dan Jagger, Jeremy Green, Michael Duchen and Gyorgy Szabadkai and Jonathan Gale for providing comments and discussion on earlier versions of the manuscript. This project was supported by funds from the King's Prize Fellowship (King's College London) (ZFM) and the Biotechnology and Biological Sciences Research Council (BBSRC) grant BB/V006371/1 (ZFM).

Author contributions

ZFM, TSB conceptualised the study and experimental design.
ZFM, TSB, JO, MA developed and executed the methodology.
ZFM, JO, VY analysed and interpreted the data.
ZFM, TSB, JO, VY wrote and edited the manuscript, which was reviewed by all contributing authors.
ZFM is the guarantor of this study, with responsibility for integrity and accuracy of the data.

1064 **References**

1065 1 Gordon-Salant, S. Hearing loss and aging: new research findings and clinical implications. *J*
1066 *Rehabil Res Dev* **42**, 9-24, doi:10.1682/jrrd.2005.01.0006 (2005).
1067 2 Fettiplace, R. & Nam, J. H. Tonotopy in calcium homeostasis and vulnerability of cochlear hair
1068 cells. *Hear Res* **376**, 11-21, doi:10.1016/j.heares.2018.11.002 (2019).
1069 3 Wu, F., Xiong, H. & Sha, S. Noise-induced loss of sensory hair cells is mediated by
1070 ROS/AMPKalpha pathway. *Redox Biol* **29**, 101406, doi:10.1016/j.redox.2019.101406 (2020).
1071 4 Forge, A. & Richardson, G. Freeze fracture analysis of apical membranes in cochlear cultures:
1072 differences between basal and apical-coil outer hair cells and effects of neomycin. *J Neurocytol*
1073 **22**, 854-867, doi:10.1007/BF01186357 (1993).
1074 5 Ito, K. & Ito, K. Metabolism and the Control of Cell Fate Decisions and Stem Cell Renewal. *Annu*
1075 *Rev Cell Dev Biol* **32**, 399-409, doi:10.1146/annurev-cellbio-111315-125134 (2016).
1076 6 Bhattacharya, D., Azambuja, A. P. & Simoes-Costa, M. Metabolic Reprogramming Promotes
1077 Neural Crest Migration via Yap/Tead Signaling. *Dev Cell* **53**, 199-211 e196,
1078 doi:10.1016/j.devcel.2020.03.005 (2020).
1079 7 Kantarci, H., Gou, Y. & Riley, B. B. The Warburg Effect and lactate signaling augment Fgf-MAPK
1080 to promote sensory-neural development in the otic vesicle. *Elife* **9**, doi:10.7554/eLife.56301
1081 (2020).
1082 8 Chi, F., Sharpley, M. S., Nagaraj, R., Roy, S. S. & Banerjee, U. Glycolysis-Independent Glucose
1083 Metabolism Distinguishes TE from ICM Fate during Mammalian Embryogenesis. *Dev Cell* **53**,
1084 9-26 e24, doi:10.1016/j.devcel.2020.02.015 (2020).
1085 9 Oginuma, M. *et al.* A Gradient of Glycolytic Activity Coordinates FGF and Wnt Signaling during
1086 Elongation of the Body Axis in Amniote Embryos. *Dev Cell* **40**, 342-353 e310,
1087 doi:10.1016/j.devcel.2017.02.001 (2017).
1088 10 Oginuma, M. *et al.* Intracellular pH controls WNT downstream of glycolysis in amniote
1089 embryos. *Nature* **584**, 98-101, doi:10.1038/s41586-020-2428-0 (2020).
1090 11 Bulusu, V. *et al.* Spatiotemporal Analysis of a Glycolytic Activity Gradient Linked to Mouse
1091 Embryo Mesoderm Development. *Dev Cell* **40**, 331-341 e334,
1092 doi:10.1016/j.devcel.2017.01.015 (2017).
1093 12 Blacker, T. S. *et al.* Separating NADH and NADPH fluorescence in live cells and tissues using
1094 FLIM. *Nat Commun* **5**, 3936, doi:10.1038/ncomms4936 (2014).
1095 13 Majumder, P., Blacker, T. S., Nolan, L. S., Duchen, M. R. & Gale, J. E. Multiphoton NAD(P)H
1096 FLIM reveals metabolic changes in individual cell types of the intact cochlea upon
1097 sensorineural hearing loss. *Sci Rep* **9**, 18907, doi:10.1038/s41598-019-55329-x (2019).
1098 14 Blacker, T., Marsh, RJ., Duchen, MR., & Bain, AJ. . Activated barrier crossing dynamics in the
1099 non-radiative decay of NADH and NADPH. . *Chem. Phys.* **422**, 184-194 (2013).
1100 15 Blacker, T. S. & Duchen, M. R. Investigating mitochondrial redox state using NADH and NADPH
1101 autofluorescence. *Free Radic Biol Med* **100**, 53-65, doi:10.1016/j.freeradbiomed.2016.08.010
1102 (2016).
1103 16 Tilney, L. G., Tilney, M. S. & DeRosier, D. J. Actin filaments, stereocilia, and hair cells: how cells
1104 count and measure. *Annu Rev Cell Biol* **8**, 257-274, doi:10.1146/annurev.cb.08.110192.001353
1105 (1992).
1106 17 Goodyear, R. & Richardson, G. Pattern formation in the basilar papilla: evidence for cell
1107 rearrangement. *J Neurosci* **17**, 6289-6301 (1997).
1108 18 Mann, Z. F. *et al.* A gradient of Bmp7 specifies the tonotopic axis in the developing inner ear.
1109 *Nat Commun* **5**, 3839, doi:10.1038/ncomms4839 (2014).
1110 19 Skala, M. C. *et al.* In vivo multiphoton microscopy of NADH and FAD redox states, fluorescence
1111 lifetimes, and cellular morphology in precancerous epithelia. *Proc Natl Acad Sci U S A* **104**,
1112 19494-19499, doi:10.1073/pnas.0708425104 (2007).

1113 20 Yu, Q. & Heikal, A. A. Two-photon autofluorescence dynamics imaging reveals sensitivity of
1114 intracellular NADH concentration and conformation to cell physiology at the single-cell level.
1115 *J Photochem Photobiol B* **95**, 46-57, doi:10.1016/j.jphotobiol.2008.12.010 (2009).
1116 21 Gafni, A. & Brand, L. Fluorescence decay studies of reduced nicotinamide adenine
1117 dinucleotide in solution and bound to liver alcohol dehydrogenase. *Biochemistry* **15**, 3165-
1118 3171, doi:10.1021/bi00660a001 (1976).
1119 22 Sanchez, T., Zhang, M., Needleman, D. & Seli, E. Metabolic imaging via fluorescence lifetime
1120 imaging microscopy for egg and embryo assessment. *Fertil Steril* **111**, 212-218,
1121 doi:10.1016/j.fertnstert.2018.12.014 (2019).
1122 23 Bradshaw, P. C. Cytoplasmic and Mitochondrial NADPH-Coupled Redox Systems in the
1123 Regulation of Aging. *Nutrients* **11**, doi:10.3390/nu11030504 (2019).
1124 24 Ge, T. *et al.* The Role of the Pentose Phosphate Pathway in Diabetes and Cancer. *Front*
1125 *Endocrinol (Lausanne)* **11**, 365, doi:10.3389/fendo.2020.00365 (2020).
1126 25 Hitosugi, T. & Chen, J. Post-translational modifications and the Warburg effect. *Oncogene* **33**,
1127 4279-4285, doi:10.1038/onc.2013.406 (2014).
1128 26 Fritz, P. J. Rabbit muscle lactate dehydrogenase 5; a regulatory enzyme. *Science* **150**, 364-366,
1129 doi:10.1126/science.150.3694.364 (1965).
1130 27 Liu, J. *et al.* Aberrant FGFR Tyrosine Kinase Signaling Enhances the Warburg Effect by
1131 Reprogramming LDH Isoform Expression and Activity in Prostate Cancer. *Cancer Res* **78**, 4459-
1132 4470, doi:10.1158/0008-5472.CAN-17-3226 (2018).
1133 28 Zhang, D. *et al.* Metabolic reprogramming of cancer-associated fibroblasts by IDH3alpha
1134 downregulation. *Cell Rep* **10**, 1335-1348, doi:10.1016/j.celrep.2015.02.006 (2015).
1135 29 Ugur, B. *et al.* The Krebs Cycle Enzyme Isocitrate Dehydrogenase 3A Couples Mitochondrial
1136 Metabolism to Synaptic Transmission. *Cell Rep* **21**, 3794-3806,
1137 doi:10.1016/j.celrep.2017.12.005 (2017).
1138 30 Yamada, K., Saito, M., Matsuoka, H. & Inagaki, N. A real-time method of imaging glucose
1139 uptake in single, living mammalian cells. *Nat Protoc* **2**, 753-762, doi:10.1038/nprot.2007.76
1140 (2007).
1141 31 Katayama, A. & Corwin, J. T. Cell production in the chicken cochlea. *J Comp Neurol* **281**, 129-
1142 135, doi:10.1002/cne.902810110 (1989).
1143 32 Barban, S. & Schulze, H. O. The effects of 2-deoxyglucose on the growth and metabolism of
1144 cultured human cells. *J Biol Chem* **236**, 1887-1890 (1961).
1145 33 Pascale, R. M., Peitta, G., Simile, M. M. & Feo, F. Alterations of Methionine Metabolism as
1146 Potential Targets for the Prevention and Therapy of Hepatocellular Carcinoma. *Medicina*
1147 *(Kaunas)* **55**, doi:10.3390/medicina55060296 (2019).
1148 34 Arnold, P. K. *et al.* A non-canonical tricarboxylic acid cycle underlies cellular identity. *Nature*
1149 **603**, 477-481, doi:10.1038/s41586-022-04475-w (2022).
1150 35 Zhong, Y. *et al.* Application of mitochondrial pyruvate carrier blocker UK5099 creates
1151 metabolic reprogram and greater stem-like properties in LnCap prostate cancer cells in vitro.
1152 *Oncotarget* **6**, 37758-37769, doi:10.18632/oncotarget.5386 (2015).
1153 36 Towers, M., Wolpert, L. & Tickle, C. Gradients of signalling in the developing limb. *Curr Opin*
1154 *Cell Biol* **24**, 181-187, doi:10.1016/j.ceb.2011.11.005 (2012).
1155 37 Averbukh, I., Ben-Zvi, D., Mishra, S. & Barkai, N. Scaling morphogen gradients during tissue
1156 growth by a cell division rule. *Development* **141**, 2150-2156, doi:10.1242/dev.107011 (2014).
1157 38 Zhao, J. *et al.* Low-dose 2-deoxyglucose and metformin synergically inhibit proliferation of
1158 human polycystic kidney cells by modulating glucose metabolism. *Cell Death Discov* **5**, 76,
1159 doi:10.1038/s41420-019-0156-8 (2019).
1160 39 Franco, B. & Malgrange, B. Concise Review: Regeneration in Mammalian Cochlea Hair Cells:
1161 Help from Supporting Cells Transdifferentiation. *Stem Cells* **35**, 551-556,
1162 doi:10.1002/stem.2554 (2017).

1163 40 Koehler, K. R., Mikosz, A. M., Molosh, A. I., Patel, D. & Hashino, E. Generation of inner ear
1164 sensory epithelia from pluripotent stem cells in 3D culture. *Nature* **500**, 217-221,
1165 doi:10.1038/nature12298 (2013).
1166 41 Cliff, T. S. & Dalton, S. Metabolic switching and cell fate decisions: implications for
1167 pluripotency, reprogramming and development. *Curr Opin Genet Dev* **46**, 44-49,
1168 doi:10.1016/j.gde.2017.06.008 (2017).
1169 42 Kolla, L. *et al.* Characterization of the development of the mouse cochlear epithelium at the
1170 single cell level. *Nat Commun* **11**, 2389, doi:10.1038/s41467-020-16113-y (2020).
1171 43 Driver, E. C. & Kelley, M. W. Development of the cochlea. *Development* **147**,
1172 doi:10.1242/dev.162263 (2020).
1173 44 Hume, C. R., Bratt, D. L. & Oesterle, E. C. Expression of LHX3 and SOX2 during mouse inner ear
1174 development. *Gene Expr Patterns* **7**, 798-807, doi:10.1016/j.modgep.2007.05.002 (2007).
1175 45 Hao, Y. *et al.* Integrated analysis of multimodal single-cell data. *Cell* **184**, 3573-3587 e3529,
1176 doi:10.1016/j.cell.2021.04.048 (2021).
1177 46 Butler, A., Hoffman, P., Smibert, P., Papalexi, E. & Satija, R. Integrating single-cell
1178 transcriptomic data across different conditions, technologies, and species. *Nat Biotechnol* **36**,
1179 411-420, doi:10.1038/nbt.4096 (2018).
1180 47 Ju, H. Q., Lin, J. F., Tian, T., Xie, D. & Xu, R. H. NADPH homeostasis in cancer: functions,
1181 mechanisms and therapeutic implications. *Signal Transduct Target Ther* **5**, 231,
1182 doi:10.1038/s41392-020-00326-0 (2020).
1183 48 Pelley, J. W. Elsevier's Integrated Review Biochemistry (Second Edition). 75-79, doi:
1184 https://doi.org/10.1016/B978-0-323-07446-9.00009-X (2012).
1185 49 Shu, Y. *et al.* Renewed proliferation in adult mouse cochlea and regeneration of hair cells. *Nat*
1186 *Commun* **10**, 5530, doi:10.1038/s41467-019-13157-7 (2019).
1187 50 Taylor, R. R. *et al.* Regenerating hair cells in vestibular sensory epithelia from humans. *Elife* **7**,
1188 doi:10.7554/eLife.34817 (2018).
1189 51 Shibata, S. B. *et al.* Gene therapy for hair cell regeneration: Review and new data. *Hear Res*
1190 **394**, 107981, doi:10.1016/j.heares.2020.107981 (2020).
1191 52 Tao, L. *et al.* Enhancer decommissioning imposes an epigenetic barrier to sensory hair cell
1192 regeneration. *Dev Cell* **56**, 2471-2485 e2475, doi:10.1016/j.devcel.2021.07.003 (2021).
1193 53 Yang, H. *et al.* SIRT3-dependent GOT2 acetylation status affects the malate-aspartate NADH
1194 shuttle activity and pancreatic tumor growth. *EMBO J* **34**, 1110-1125,
1195 doi:10.15252/embj.201591041 (2015).
1196 54 Dong, G. *et al.* PKM2 and cancer: The function of PKM2 beyond glycolysis. *Oncol Lett* **11**, 1980-
1197 1986, doi:10.3892/ol.2016.4168 (2016).
1198 55 Kotowski, K. *et al.* Role of PFKFB3 and PFKFB4 in Cancer: Genetic Basis, Impact on Disease
1199 Development/Progression, and Potential as Therapeutic Targets. *Cancers (Basel)* **13**,
1200 doi:10.3390/cancers13040909 (2021).
1201 56 Yi, M. *et al.* 6-Phosphofructo-2-kinase/fructose-2,6-biphosphatase 3 and 4: A pair of valves for
1202 fine-tuning of glucose metabolism in human cancer. *Mol Metab* **20**, 1-13,
1203 doi:10.1016/j.molmet.2018.11.013 (2019).
1204 57 Vander Heiden, M. G., Cantley, L. C. & Thompson, C. B. Understanding the Warburg effect: the
1205 metabolic requirements of cell proliferation. *Science* **324**, 1029-1033,
1206 doi:10.1126/science.1160809 (2009).
1207 58 Vizan, P. *et al.* Modulation of pentose phosphate pathway during cell cycle progression in
1208 human colon adenocarcinoma cell line HT29. *Int J Cancer* **124**, 2789-2796,
1209 doi:10.1002/ijc.24262 (2009).
1210 59 A, R. J. *et al.* Cell-size dependent progression of the cell cycle creates homeostasis and
1211 flexibility of plant cell size. *Nat Commun* **8**, 15060, doi:10.1038/ncomms15060 (2017).

1212 60 Kaplon, J., van Dam, L. & Peeper, D. Two-way communication between the metabolic and cell
1213 cycle machineries: the molecular basis. *Cell Cycle* **14**, 2022-2032,
1214 doi:10.1080/15384101.2015.1044172 (2015).
1215 61 Dessaud, E., McMahon, A. P. & Briscoe, J. Pattern formation in the vertebrate neural tube: a
1216 sonic hedgehog morphogen-regulated transcriptional network. *Development* **135**, 2489-2503,
1217 doi:10.1242/dev.009324 (2008).
1218 62 Sagner, A. & Briscoe, J. Establishing neuronal diversity in the spinal cord: a time and a place.
1219 *Development* **146**, doi:10.1242/dev.182154 (2019).
1220 63 Son, E. J. *et al.* Conserved role of Sonic Hedgehog in tonotopic organization of the avian basilar
1221 papilla and mammalian cochlea. *Proc Natl Acad Sci U S A* **112**, 3746-3751,
1222 doi:10.1073/pnas.1417856112 (2015).
1223 64 Spannl, S. *et al.* Glycolysis regulates Hedgehog signalling via the plasma membrane potential.
1224 *EMBO J* **40**, e107925, doi:10.15252/embj.2021107925 (2021).
1225 65 Gleich, O., Dooling, R. J. & Manley, G. A. Audiogram, body mass, and basilar papilla length:
1226 correlations in birds and predictions for extinct archosaurs. *Naturwissenschaften* **92**, 595-598,
1227 doi:10.1007/s00114-005-0050-5 (2005).
1228 66 Belanger, M., Allaman, I. & Magistretti, P. J. Brain energy metabolism: focus on astrocyte-
1229 neuron metabolic cooperation. *Cell Metab* **14**, 724-738, doi:10.1016/j.cmet.2011.08.016
1230 (2011).
1231 67 Majumder, P., Duchen, M. R. & Gale, J. E. Cellular glutathione content in the organ of Corti
1232 and its role during ototoxicity. *Front Cell Neurosci* **9**, 143, doi:10.3389/fncel.2015.00143
1233 (2015).
1234 68 Fetoni, A. R. *et al.* Cx26 partial loss causes accelerated presbycusis by redox imbalance and
1235 dysregulation of Nfr2 pathway. *Redox Biol* **19**, 301-317, doi:10.1016/j.redox.2018.08.002
1236 (2018).
1237 69 Driver, E. C., Sillers, L., Coate, T. M., Rose, M. F. & Kelley, M. W. The Atoh1-lineage gives rise
1238 to hair cells and supporting cells within the mammalian cochlea. *Dev Biol* **376**, 86-98,
1239 doi:10.1016/j.ydbio.2013.01.005 (2013).
1240 70 Jacques, B. E. *et al.* The role of Wnt/beta-catenin signaling in proliferation and regeneration
1241 of the developing basilar papilla and lateral line. *Dev Neurobiol* **74**, 438-456,
1242 doi:10.1002/dneu.22134 (2014).

1243
1244
1245